

Reconstructing the late Pleistocene climate  
sequence at Alexandra Cave, Naracoorte,  
South Australia, using single-grain Optically  
Stimulated Luminescence dating and  
palaeoenvironmental proxies

Thesis submitted in accordance with the requirements of the University of Adelaide  
for an Honours Degree in Environmental Geoscience

Priya

October 2018



THE UNIVERSITY  
*of* ADELAIDE

# **RECONSTRUCTING THE LATE PLEISTOCENE CLIMATE SEQUENCE AT ALEXANDRA CAVE, NARACOORTE, USING SINGLE-GRAIN OPTICALLY STIMULATED LUMINESCENCE DATING AND PALAEOENVIRONMENTAL PROXIES**

## **RUNNING TITLE: OSL AND PALAEOENVIRONMENTAL PROXIES IN ALEXANDRA CAVE, NARACOORTE**

### **ABSTRACT**

The drivers of the Australia-wide megafaunal extinction during the late Pleistocene remains poorly resolved. Hypotheses include individual or synergistic combinations of climate fluctuations, human impacts through hunting or habitat alteration by landscape burning. Moreover, the relationship between extinction dynamics and long term glacial - interglacial timescales is not yet understood. Using a series of complementary geochronology, palaeoecological and geochemical techniques on a sedimentary sequence in Alexandra Cave, Naracoorte, this study provides improved reconstructions of past climates in south-east South Australia around the time of megafaunal extinction. Ten luminescence dating samples constrain the age of the sedimentary sequence to 17.7 – 106.3 ka. Palaeoenvironmental reconstructions undertaken using charcoal, carbon isotopes and geochemical analysis reveal high fire frequency and precipitation during Marine Isotope Stage (MIS) 5, while MIS 4 and the Last Glacial Maximum were arid, with low fire frequency. MIS 3 was wet, with little fluctuation in the environment, with the exception of a change in biomass burning at 36 – 50 ka. These findings suggest that climate change likely played a minor role in the demise of megafauna locally, whereas changes in fire regime could have acted as a more significant driver or consequence of megafauna extinction.

### **KEYWORDS**

Luminescence dating, charcoal, pollen, *Sporormiella*, Alexandra Cave, Naracoorte, megafauna extinction

## TABLE OF CONTENTS

|  |    |
|--|----|
| List of Figures and Tables .....                                   | 5  |
| Introduction .....   | 6  |
| Background .....   | 10 |
| Study site.....  | 10 |
| Single-grain Optically Stimulated Luminescence dating .....        | 13 |
| Charcoal.....  | 15 |
| Pollen.....  | 16 |
| <i>Sporormiella</i> .....  | 16 |
| Carbon isotopes.....   | 17 |
| Geochemistry.....  | 18 |
| Methods .....  | 20 |
| Stratigraphic analysis.....  | 20 |
| Single-grain Optically Stimulated Luminescence dating .....        | 20 |
| Charcoal, pollen and <i>Sporormiella</i> .....                     | 21 |
| Carbon isotopes.....   | 21 |
| Geochemistry.....  | 22 |
| Results .....  | 23 |
| Stratigraphic analysis.....  | 23 |
| Geochronology .....  | 26 |
| Charcoal.....  | 34 |
| Pollen & <i>Sporormiella</i> .....                                 | 36 |
| Carbon isotopes.....   | 37 |
| Geochemistry.....  | 38 |
| Discussion .....   | 40 |
| Geochronology .....  | 40 |
| Fire history .....   | 42 |
| Palaeovegetation.....  | 43 |
| Geochemistry.....  | 45 |
| Palaeoenvironmental reconstruction and regional associations ..... | 47 |
| Marine Isotope Stage 5 (123 – 71 ka) .....                         | 47 |
| Marine Isotope Stage 4 (71 – 57 ka).....                           | 49 |
| Marine Isotope Stage 3 (57 – 29 ka).....                           | 49 |
| The Last Glacial Maximum (29 – 17 ka).....                         | 50 |
| Implications for the megafaunal extinction debate .....            | 51 |

|   |    |
|---|----|
| Future directions.....                                      | 53 |
| Conclusion.....   | 55 |
| Acknowledgements .....                                      | 57 |
| References.....   | 58 |
| Appendix .....  | 65 |
| Appendix 1: Radiocarbon ages from Alexandra Cave .....      | 65 |
| Appendix 2: OSL sampling in field .....                     | 66 |
| Appendix 3: OSL sample procedure .....                      | 67 |
| Appendix 4: OSL equipment setting.....                      | 68 |
| Appendix 5: Single-Aliquot Regenerative (SAR) Protocol..... | 69 |
| Appendix 6: Bayesian age-depth model.....                   | 70 |
| Appendix 7: Pollen sample procedure.....                    | 71 |
| Appendix 8: Macro-charcoal set-up.....                      | 72 |
| Appendix 9: ITRAX™ XRF core scanning .....                  | 73 |
| Appendix 10: Micro- and macro fraction data.....            | 74 |
| Appendix 11: Carbon isotope data.....                       | 76 |

## List of Figures and Tables

|   |    |
|---|----|
| Figure 1: Conceptual diagram of project aims .....                                | 11 |
| Figure 2: Map of Alexandra Cave in context of Australia .....                     | 14 |
| Figure 3: Field photos of sedimentary section in Alexandra Cave .....             | 34 |
| Figure 4: Stratigraphic log of Alexandra Cave sediment sequence .....             | 35 |
| Figure 5: Multi-aliquot dose recovery test .....                                  | 26 |
| Figure 6a: Radial plot and histogram of ALEX 18-1 to ALEX 18-5 .....              | 29 |
| Figure 6b: Radial plot and histogram of ALEX 18-6 to ALEX 18-10 .....             | 30 |
| Figure 7: Age-depth profile of OSL and radiocarbon ages .....                     | 32 |
| Figure 8: Micro-charcoal and macro-charcoal fraction with depth .....             | 37 |
| Figure 9: Linear regression performed on micro and macro-charcoal fractions ..... | 38 |
| Figure 10: Stable carbon isotopes with depth .....                                | 39 |
| Figure 11: XRF core scanning of elements against depth .....                      | 41 |
| Figure 12: Alexandra Cave in context of Naracoorte Caves National Park.....       | 44 |
| Figure 13: Summary plot of proxies with regional comparison .....                 | 48 |
| <br>  |    |
| Table 1: Elemental ratios of interest for XRF core scanning .....                 | 22 |
| Table 2: Single-grain dose recovery test .....                                    | 27 |
| Table 3: Summary statistics of OSL age components .....                           | 31 |
| Table 4: Sedimentation rates of Alexandra Cave sequence.....                      | 32 |

## INTRODUCTION

Australia experienced a continent-wide extinction of approximately 85% of ‘megafauna’ (large mammals > 44 kg) during the late Pleistocene (36.7 – 48.1 ka) (Ayliffe, 1998; Price et al., 2017; Saltré et al., 2016). Identifying the key drivers of this extinction is controversial because it occurred soon after human arrival (55.4 – 55.7 ka) (Saltré et al., 2016; van der Kaars et al., 2017), yet there is presently no widespread evidence for predation or consumption of megafauna by early humans, despite coexisting for 13.5 ka (Hamm et al., 2016; Saltré et al., 2016; Wroe et al., 2013). Possible causes of extinction include individual or synergistic combinations of climate fluctuations, human impacts through hunting or habitat alteration by landscape burning (Brook et al., 2007; Lopes dos Santos et al., 2013). However, understanding the megafaunal extinction in relation to broader environmental changes, and repeated climate change still remains unresolved (Rule et al., 2012). A scarcity of stratigraphically well-constrained fossil sites found in association with high-resolution palaeoenvironmental records is a major contributing factor that limits the extent to which this highly-debated topic can be addressed (Roberts et al., 2001).

The Naracoorte Caves National Park (NCNP) is a World Heritage site known for its rich megafaunal deposits and sediment infill sequences that span the last 500 thousand years (ka) (Reed & Bourne, 2000). Alexandra Cave is one of the few sites at NCNP with a spatially continuous infill sequence that potentially contains several high-resolution palaeoenvironmental proxies that can be directly correlated to megafaunal fossil assemblages. The chronology and sediment infilling dynamics of the site remains poorly resolved. A preliminary radiocarbon dating study constrained the top 2 meters (m) of the sequence to 18 – 31 ka (McCluskey, 2012). Beneath this, another 2 m of sediment is yet to be dated, and

extends beyond the reliable limits of radiocarbon dating (McCluskey, 2012). The presence of megafauna fossils suggests that this section overlaps the megafaunal extinction window (Reed & Bourne, 2000). If so, the palaeoenvironmental sequence in Alexandra Cave could potentially provide new insights into the driving forces behind the controversial megafaunal extinction and broader long-term environmental changes.

The overarching aim of this thesis is to provide improved reconstructions of past climates and palaeoenvironmental conditions in NCNP around the time of megafaunal extinction using a series of complementary geochronology, palaeoecological and geochemical techniques. This will be achieved through the following specific aims:

- (1) Undertake refined stratigraphic assessments of the Alexandra Cave sediment sequence.
- (2) Establish a detailed chronology for the sequence using single-grain Optically Stimulated Luminescence (OSL) dating of sedimentary quartz grains.
- (3) Analyse the local and regional fire history by examining macro- and micro- charcoal with a focus on Marine Isotope Stage (MIS) 3 – 5 (29 – 130 ka).
- (4) Reconstruct past vegetation records from taphonomic analysis and relative abundance assessments of pollen during the critical MIS 3 – 5 timeframe.
- (5) Obtain pilot data on the preservation of dung spores (*Sporormiella*) within the MIS 3 – 5 part of the sequence and explore its usefulness as a proxy for megaherbivore presence.

- (6) Analyse carbon isotopes ( $\delta^{13}\text{C}$ ) of charcoal as an indication of moisture in the environment.
- (7) Evaluate geochemical changes in palaeoenvironmental conditions and sedimentary infilling dynamics using high-resolution X-Ray Fluorescence (XRF) sediment scanning.

The multiple components of this project are conceptualised in Figure 1. The multi-proxy study is designed around several independent lines of evidence that can help evaluate and resolve the aforementioned hypotheses (e.g. Birks & Birks, 2006). Each proxy examined in this study reflects the environment at its own spatial scale, and provides a different insight into past environments. Paired with reliable geochronology, it is hoped that this project can provide improved reconstructions of late Pleistocene climate and environments at NCNP.



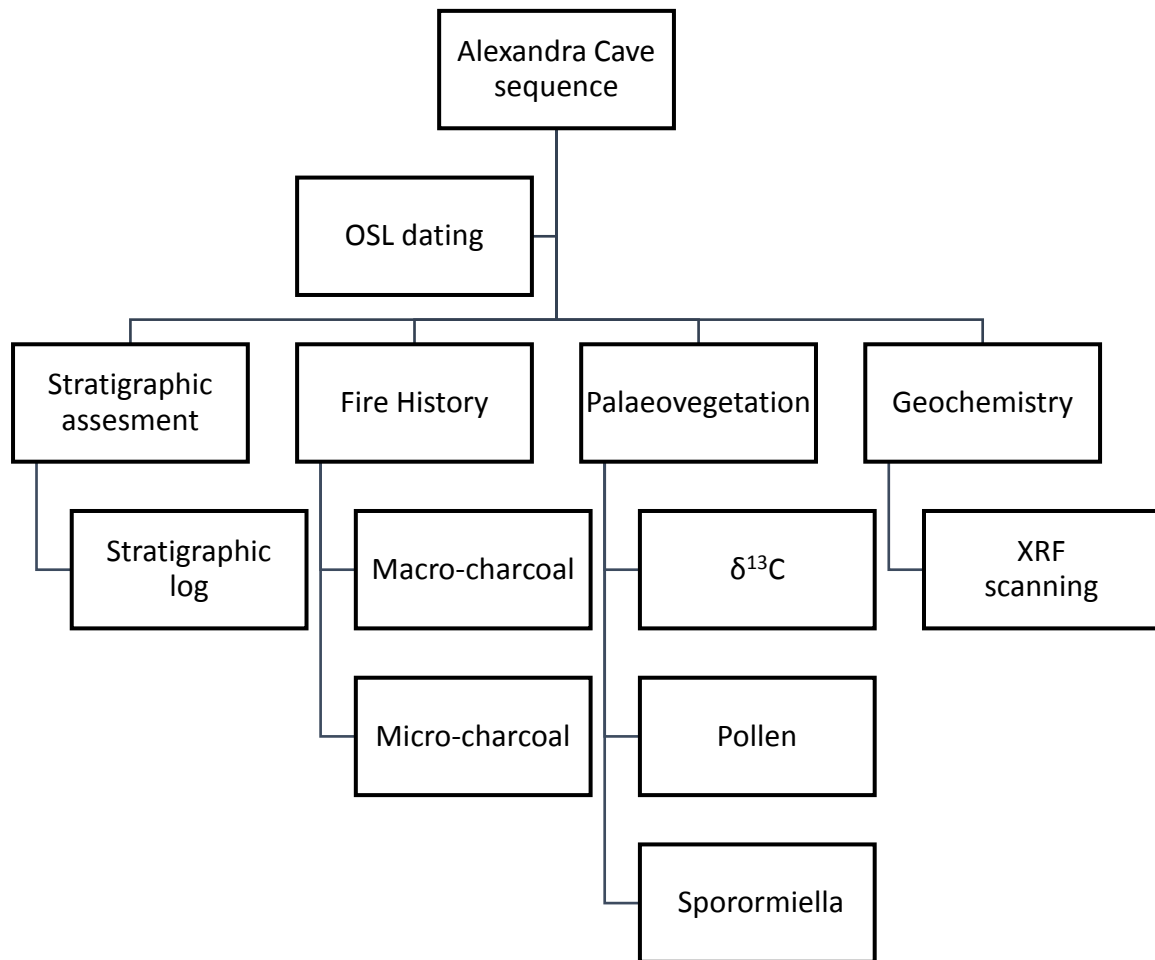


Figure 1. Conceptual diagram of multi-proxy approach to address the project aims of reconstructing past environments in NCNP.

## BACKGROUND

### Study site

The Naracoorte Caves National Park (NCNP) is part of the southeast karst province of South Australia, and consists of Eocene to Miocene Gambier Limestone (White & Webb, 2015).

The Naracoorte cave complex developed via phreatic dissolution in the Naracoorte Member of the Gambier Limestone during the early Pleistocene (White & Webb, 2015). Since then, these caves have been in the vadose zone, and allochthonous sedimentation of the cavities has been dominated by surface run-off, colluvial and alluvial processes (Forbes & Bestland, 2007).

Alexandra Cave (Australian Karst register 5U3) is one of 26 caves in NCNP that receives up to 18,000 visitors annually (Adetutu et al., 2012). There are four main chambers connected by low passages, and infilled with silt- and sand-sized deposits (Reed & Bourne, 2000). Since its discovery in 1908, the naturally sealed original solution tube entrance has been extensively modified, and a new artificial entrance has since been excavated for tourists (Department for Environment and Heritage, 2001). In the process of excavation, a 5 m thick sedimentary sequence was exposed in the entrance chamber that appears to be laterally continuous for 30 m (Figure 2). Megafauna fossils recovered during the excavation include *Thylacoleo carnifax*, a marsupial lion, and two genera of short-faced kangaroos, *Procoptodon goliath* and *Simostenurus* (Reed & Bourne, 2000).

An initial study of the cave sediment infill history was undertaken by McCluskey (2012), exploring grain-size, grain morphology, sediment source, geochemistry and geochronology of the Alexandra Cave sequence. The sediments were interpreted to be alluvial and colluvial in

source based on their bimodal grain-size distribution. The large peak grain-size observed throughout the sequence (200 – 300  $\mu\text{m}$ ) was taken to be indicative of a high-energy depositional environment. Geochemical tracing of sediment origin yielded inconclusive results. Four radiocarbon ages were obtained on degraded charcoal, constraining the top 2 m of the sedimentary sequence to 18 – 32 ka (Appendix 1). However, two of these ages (Sample A4 = 27 286 – 27 690 cal yr. BP and sample B8 = 29 830 – 30 826 cal yr. BP) were considered to be unreliable due to low carbon content (16 – 17%), and therefore likely represent minimum ages for the infill sequence (McCluskey, 2012). An additional 2 m of sediment found below the section studied by McCluskey (2012) has yet to be dated, and likely extends beyond the reliable limits of radiocarbon dating.

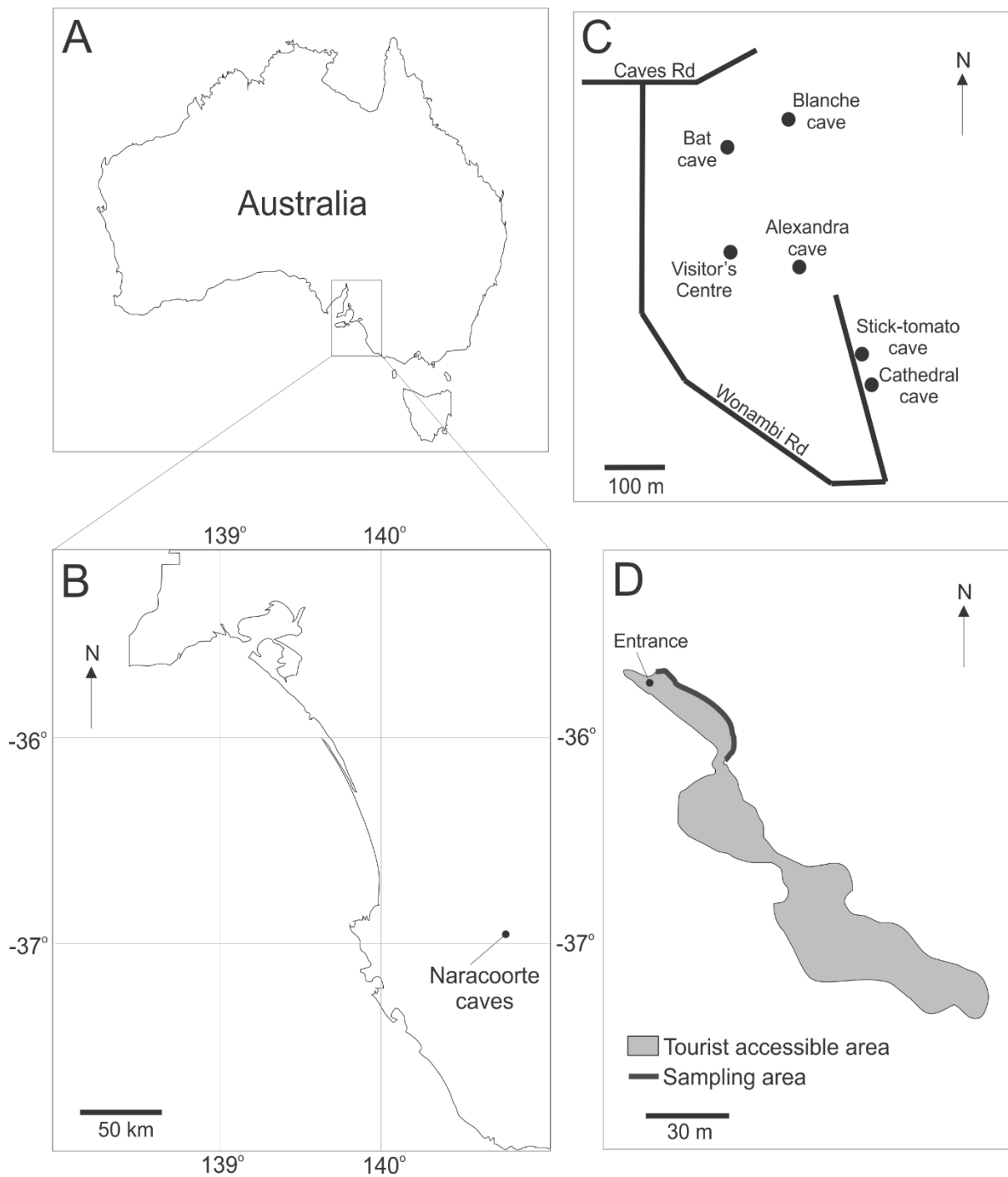


Figure 2. Location of Alexandra cave: A. Map of Australia B. The south-eastern region of South Australia with location of Naracoorte Caves C. Naracoorte Caves National Park showing the location of Alexandra Cave (-37.0347, 140.795) D. Alexandra Cave chamber indicating sampling area (adapted from Reed, 2018).

### **Single-grain Optically Stimulated Luminescence dating**

Optically Stimulated Luminescence (OSL) dating is a widely used method for constraining the depositional age of late Pleistocene sediments that contain abundant silicate minerals (Aitken., 1998; Huntley et al., 1985). The dating procedure itself can be labour intensive, time consuming and costly (Nelson et al., 2017). The sedimentary sequence in Alexandra Cave is predominantly composed of quartz grains (McCluskey, 2012), making OSL an ideal dating method for this sequence.

OSL dating involves the measurement of light-sensitive trapped charges within grains to determine the time since these minerals were last exposed to daylight (Aitken, 1985). Over time, when grains are buried and no longer exposed to daylight, charge populations begin to accumulate at localised defect sites within the crystal lattice, as a result of absorption of ionizing radiation from surrounding sediment and cosmic rays (Galbraith & Roberts, 2012). The accumulation of charge throughout the burial period occurs at a rate proportional to the natural surrounding radioactivity (Aitken, 1998). An OSL age is calculated by estimating the (1) equivalent dose ( $D_e$ ) within a quartz grain since burial and (2) the natural environmental dose rate (Aitken, 1998).

The  $D_e$  represents the laboratory estimate of the natural radiation dose absorbed by the sample during burial (Galbraith & Roberts, 2012). To calculate the  $D_e$  for a sample, the Single-Aliquot Regenerative (SAR) method is used where a dose-response curve is constructed after first measuring and removing the natural signal, then adding known doses to each grain. A preheat is also added to account for any signal sensitivity changes during repeated heating and irradiation, and to remove any thermally unstable charge contributions from the measured OSL signals. The  $D_e$  value is calculated by interpolating the sensitivity-corrected

natural OSL signal onto a dose-response curve obtained by administering a series of known doses to the sample using a calibrated laboratory radiation source (Murray & Wintle, 2000).

A key advancement in OSL dating has been the development of single-grain OSL techniques, where  $D_e$  values are measured for individual grains rather than multi-grain aliquots, which can contain up to several hundreds of grains (Galbraith & Roberts, 2012). Single-grain  $D_e$  distributions provide greater insight into the luminescence properties of grains that might otherwise be overlooked with multi-grain aliquots. Using single-grain analyses can differentiate post-depositionally mixed grain populations and partially bleached samples (i.e., samples that have not been exposed to prolonged daylight prior to burial) (Jacobs & Roberts, 2008). This improved technique is particularly useful in archaeological and palaeontological sites, where a more representative  $D_e$  value can be estimated from complex datasets (Arnold & Demuro, in press).

To derive the environmental dose rate, external gamma and beta dose rates are measured from the surrounding sediment matrix using a field gamma spectrometer and beta counter, respectively (Arnold et al., 2013). The internal dose rate of the measured grains is calculated using an electron microprobe or inductively coupled plasma mass spectrometry (ICP-MS) analysis. The cosmic dose rates are determined using empirical equations that take into consideration altitude, geomagnetic latitude and thickness of sediment and bedrock overburden (Prescott & Hutton, 1995). According to Galbraith and Roberts (2012), in its simplest form, the OSL age (i.e. time since burial) is derived using the following equation:

$$\text{Age (ka)} = \frac{\text{Equivalent dose (De)}}{\text{Environmental Dose rate}} \frac{\text{Gy}}{(\text{Gy/Ka})}$$

## **Charcoal**

Stratigraphic charcoal analysis is widely used as a proxy for past fire history (Clark & Hussey, 1996). Water and wind are the primary sources of charcoal in sediment depositions (Crawford & Belcher, 2014). By virtue of size, larger charcoal fragments tend to be transported over short distances and as a result, are an indication of a localised fire event. Smaller particles on the other hand, have low ratios of volume-to-surface area and can be transported over longer distances, indicating regional fire history (Clark, 1988). Charcoal particles  $<100\ \mu\text{m}$  are considered micro-charcoal, while  $>200\ \mu\text{m}$  particles are classed as macro-charcoal (Lynch et al., 2004). By analysing both charcoal fractions in tandem from the Alexandra Cave sediment sequence it should, in theory, be possible to reconstruct a more comprehensive fire history of the surrounding landscape.

A compilation of 223 sedimentary charcoal records from Australasia showed no distinct change in fire regime corresponding to human arrival in the region (Mooney et al., 2011). Charcoal has previously been observed alongside pollen in Blanche Cave, but not quantified (Darrénougué et al., 2009). The continuous bands of macro-charcoal observed throughout the sequence in Alexandra Cave (McCluskey, 2012), could potentially provide a high-resolution record of fire history in NCNP and southeast Australia. Placing the Alexandra Cave charcoal record into a regional context can further reveal whether the sediment deposit reflects internal cave dynamics or broader environmental changes in the region.

## **Pollen**

Fossil pollen preserved in the sedimentary record provides a potentially invaluable means of reconstructing the palaeovegetation history of a region (van der Kaars, 1991). Pollen can be dispersed in the environment and accumulates in cave infill deposits through wind, animals or through secondary processes such as debris flow (Hunt & Fiacconi, 2018). From the pollen record of Alexandra Cave, it should be possible to infer palaeoenvironmental and palaeoclimatic changes in the region, which may provide a better understanding of environmental changes around the megafauna extinction window (e.g., Rule et al., 2012; van der Kaars et al., 2017).

Pollen analysis undertaken elsewhere in NCNP at Blanche Cave documented a transition from woody taxa at the onset of the Last Glacial Maximum (LGM) to a woody-herbaceous taxa during the LGM (Darrénougué et al., 2009). Across the broader southeast South Australia region, pollen records from Lake Leake and Wylie Swamp have shown a dominance of herbaceous vegetation before and during the LGM, suggesting dry conditions at this time (Dodson, 1975; Dodson 1977). Similarly, a pollen study by Johnson et al. (2015) from Caledonia Fen in southeast Australia, showed no change in low grass/shrubland over the megafauna extinction period.

## ***Sporormiella***

*Sporormiella* is a spore of fungus found in the dung of herbivores across a wide range of body sizes (Davis, 2017). In western North America, *Sporormiella* has been established as a reliable proxy for megafaunal biomass in late Pleistocene sediments because spore counts are most strongly affected by the activity of large herbivores (Rule et al., 2012). This proxy has played a critical role in determining herbivore population crashes during the late Quaternary



in North America, Madagascar and New Zealand (Baker et al., 2013; Burney et al., 2003; Wood et al., 2011). However, in Australia the source of *Sporormiella* spores in sediment sequences and their correlation to extinct megaherbivores has not been well-documented (Dodson & Field, 2017). To date, only four sites in Australia have documented the presence of *Sporormiella* - Lynch's Crater, Cuddie Springs, Caledonia Fen and Cape Pasley marine core (Dodson & Field, 2017; Rule et al., 2012; Johnson et al., 2015; van der Kaars et al., 2017). The reported occurrences of *Sporormiella* are either sporadic or have only been found where there is no known megafauna remains (Dodson & Field, 2017). The present study therefore aims to obtain pilot spore data from the sedimentary sequence in Alexandra Cave to provide better information on *Sporormiella* preservation in cave settings, and to further investigate the potential of *Sporormiella* as a proxy for megafauna.

### **Carbon isotopes**

Stable carbon isotopes of terrestrial plants is a useful measure of moisture conditions in the environment (Diefendorf et al., 2010). Plant stomatal conductance is the measure of the rate of carbon dioxide entering or water vapour exiting through the stomatal leaf. The plant stomatal conductance decreases to minimise water loss when water availability in the environment is low. This decreases the discrimination of heavier  $^{13}\text{C}$  relative to  $^{12}\text{C}$  (Diefendorf et al., 2010).  $\text{C}_4$  plants have  $\delta^{13}\text{C}$  values that lie within the range of -9 to -16 ‰. While  $\text{C}_3$  plants have values ranging from -22 to -33‰ and are more common throughout Australia (Turney, 2012). In the absence of plant macrofossils, other material like charcoal, shells and leaf waxes can be measured for carbon isotopes (Turney et al., 2006). Owing to the abundance of charcoal observed in Alexandra Cave (McCluskey, 2012), this study focuses on measuring  $\delta^{13}\text{C}$  of charcoal rather than plant macrofossils.

## **Geochemistry**

The geochemistry of sedimentary sequences can help better understand depositional events and any unconformities or post-depositional alterations that might have occurred (Forbes & Bestland, 2007). Interpreting geochemical and lithological changes in tandem can be crucial for the reconstruction of reliable depositional histories in complex cave settings (Forbes et al., 2007).

X-Ray Fluorescence (XRF) is based on excitation of electrons by incident x-radiation. When electrons are ejected from their inner atomic shells, shell vacancies are created which are filled by electrons falling back from the outer shell. The fluorescence energy produced is characteristic of different elements, and the intensity of each emission wavelength is related to elemental concentration (Weltje & Tjallingii, 2008).

In spite of the advantages of XRF analysis, obtaining samples from large sedimentary sequences, like Alexandra Cave, can be both destructive and expensive. A complementary and novel method to reduce analytical costs and sample destruction is XRF scanning. An XRF scanner is capable of measuring sediment sections by scanning and obtaining data directly at the surface, with minimal sample preparation and destruction (Croudace & Rothwell, 2015). Additionally, the scanner can measure elemental changes at a significantly higher spatial resolution (i.e. 200  $\mu\text{m}$ ) compared to conventional XRF methods, providing a continuous, high-resolution elemental record.

The XRF scanner characterises the elements present according to their relative intensities (Weltje & Tjallingii, 2008). Quantifying the elemental intensities produced by the XRF scanner in terms of elemental concentrations can be complicated; particularly as the

conversion is not linear due to elemental interaction, variable water content and specimen homogeneity. As a result, XRF scanning data is widely accepted to be semi-quantitative (Weltje & Tjallingii, 2008). Recent studies have shown that using the log-ratios to convert elemental intensities to concentrations is the most effective method of quantifying sedimentary elements (Weltje & Tjallingii, 2008).

XRF analysis of a suite of elements can allow various inferences about the depositional environment. Table 1 summarises the suite of elements that have been used to make environmental inferences in the present study, which is based on XRF scanner studies undertaken in similar contexts around the world (Forbes & Bestland, 2007; Guyard et al., 2007; Burnett et al., 2011; Jouve et al., 2013; Croudace & Rothwell, 2015). Al, K and Si are used as indicators of sediment provenance. Fe is an indicator of reducing conditions or clay minerals. P and Ca ratios are indicative of bat guano, while S can be taken as indication of the presence of gypsum (Forbes et al., 2007; Croudace & Rothwell, 2015). The coherent and incoherent scatter values are dependent on the atomic mass of elements in the sediment (organic matter is lower than silicate minerals). Hence an increase in the inc/coh ratio can be used as an indicator of higher proportions of organic material (Burnett et al., 2011).

Table 1. Elemental ratios of interest and their respective application (Burnett et al., 2011; Croudace & Rothwell, 2015; Forbes & Bestland, 2007; Guyard et al., 2007; Jouve et al., 2013).

| <b>Elements/ ratio</b>                      | <b>Application &amp; Interpretation</b>   |
|---|---|
| Aluminium (Al), Potassium (K), Silicon (Si) | Provenance                                |
| Iron (Fe)                                   | Presence of clay minerals and iron oxides |
| Calcium (Ca), Phosphorus (P), Sulphur (S)   | Bat guano and limestone decomposition     |
| Incoherent/coherent scatter                 | Organic matter                            |

## **METHODS**

### **Stratigraphic analysis**

Grain size, sedimentary structures and sediment colour were characterised in the field using a grain size chart and Munsell Soil Colour Chart (Blott & Pye, 2012; Munsell, 2010).

Information was collected from six individual sections that were superimposed and correlated to construct a composite stratigraphic log. High-resolution images of the sedimentary sequence were also taken, aligned using photogrammetry software, Agisoft PhotoScan Professional Edition 1.4.3, and used as an aid for interpretation and correlations.

### **Single-grain Optically Stimulated Luminescence dating**

Ten luminescence dating samples were collected by placing opaque metal cylinders horizontally into cleaned surfaces and undisturbed stratigraphic layers of each unit. Each sample was selected to ensure sufficient spacing throughout the sequence, and to pick up any changes in sedimentation rate and stratigraphic units (Appendix 2). Samples were obtained and transported in light-proof packaging. Field gamma-ray spectrometry measurements were made in each sample location to derive the environmental gamma dose rate. OSL sample preparation and measurements were made on the 212 – 250 µm quartz fraction in the Prescott Environmental Luminescence Laboratory at the University of Adelaide. Detailed laboratory procedures are outlined in Appendix 3. Appropriate preheat temperatures were first determined with multi-aliquot dose-recovery test measurements, followed by single-grain dose recovery tests (to confirm the appropriateness of the chosen preheat conditions at the single-grain scale of analysis) and single-grain  $D_e$  measurements. All equipment settings are outlined in Appendix 4. Individual measured grains were subject to a series of standard quality-assurance criteria presented in Appendix 5 (Arnold et al., 2008; Arnold et al., 2013;

Arnold et al., 2016). Sedimentation rates were derived from a Bayesian age-depth model in the 'Bacon' software in R (Blaauw & Christen, 2011) (Appendix 6).

### **Charcoal, pollen and *Sporormiella***

Subsamples were collected from cleaned surfaces, with a focus on the bottom 2 m of the sedimentary profile in an attempt to capture the speculated megafaunal extinction window. A total of fifty 2 cm<sup>3</sup> samples were obtained and analysed for macro-charcoal, micro-charcoal, pollen and *Sporormiella* in the sedimentary laboratory at the University of Adelaide. Samples were sieved at 250 µm. The <250 µm fraction was analysed for pollen, *Sporormiella* and micro-charcoal using a modified protocol from Moore & Webb (1978). A detailed laboratory procedure is outlined in Appendix 7. Samples were mounted on slides and counted per 30 lycopodium grains under a Leica optical microscope at 200x magnification. Micro-charcoal is represented by particles per cm<sup>3</sup>. The >250 µm fraction was analysed for macro-charcoal. Each sample was imaged and represented as mm<sup>2</sup> per cm<sup>3</sup> in ImageJ (Schneider et al., 2012). Macro-charcoal imaging set up is outlined in Appendix 8.

### **Carbon isotopes**

Three individual charcoal pieces were picked and imaged together with a bulk charcoal sample at each luminescence sample site for <sup>13</sup>C/<sup>12</sup>C isotope ratio measurements. Samples were freeze-dried and weighed into silver capsules. The capsules were combusted in a Eurovector elemental analyser, then transported to a Nu Horizon isotope-ratio mass spectrometer. Glycine (δ<sup>13</sup>C: -31.2‰), glutamic acid (δ<sup>13</sup>C: -16.72‰) and graphite (δ<sup>13</sup>C = -16.05‰) were used as standards for calibration. δ<sup>13</sup>C values are reported in parts per mil relative to the Vienna Pee Dee Belemnite standard (VPDB).

## **Geochemistry**

A total of nine sediment cores were obtained to span the entire 3.9 m of cave sediment accumulation. High-resolution elemental analysis of the cores were obtained using the ITRAX<sup>TM</sup> Micro X-Ray Fluorescence Core Scanner at the Australian Nuclear Science and Technology Organisation (ANSTO). ITRAX<sup>TM</sup> settings for each core are presented in Appendix 9. A centered log-ratio (clr) transformation was performed and counts were normalised against stable element Ti, to account for the semi-quantitative XRF counts and effects of changing organic matter (Grant et al., 2017; Weltje & Tjallingii, 2008).

## RESULTS

### Stratigraphic analysis

The total height of the sequence is 3.9 m, with seven distinct stratigraphic units identified based on sedimentary structures, unconformities, colour classification and grain size (Figure 3). OSL samples were selected to envelope each stratigraphic unit evenly, while proxy sampling focused on sections D – F. Stratigraphic Units A – D are characterised by beige medium sand-sized sediment with well-defined parallel laminations. Section E is a 110 cm reddish-brown sediment layer, with thick sediment bedding of (>5 cm). Stratigraphic Unit F is characterised by dark black and red intermittent sediment layers that contain white nodules. Section G is a sandy-orange layer with dark mineral bandings. A detailed stratigraphic log of the stratigraphic units and sampling location is provided in Figure 4. A section of the sequence appears to be disrupted by an in-wash channel.

The overall spatial morphology and sedimentary features (parallel laminations) of the sediment deposit suggests that the sediment is primarily part of a distal cone deposit. The palaeo-entrance for Alexandra Cave is likely to be behind the exposed sedimentary surface (Figure 3), and is out of sight, making deducing of the cave entrance type difficult (Reed, personal communication, 2018).





Figure 3. Field photos of sedimentary section in Alexandra Cave. Sedimentary units are shown in each image and characterised based on sedimentary structures, unconformities, colour classification and grain size. Flame structures, charcoal bands, parallel laminations and bioturbation of the sequence are shown in the top left image.



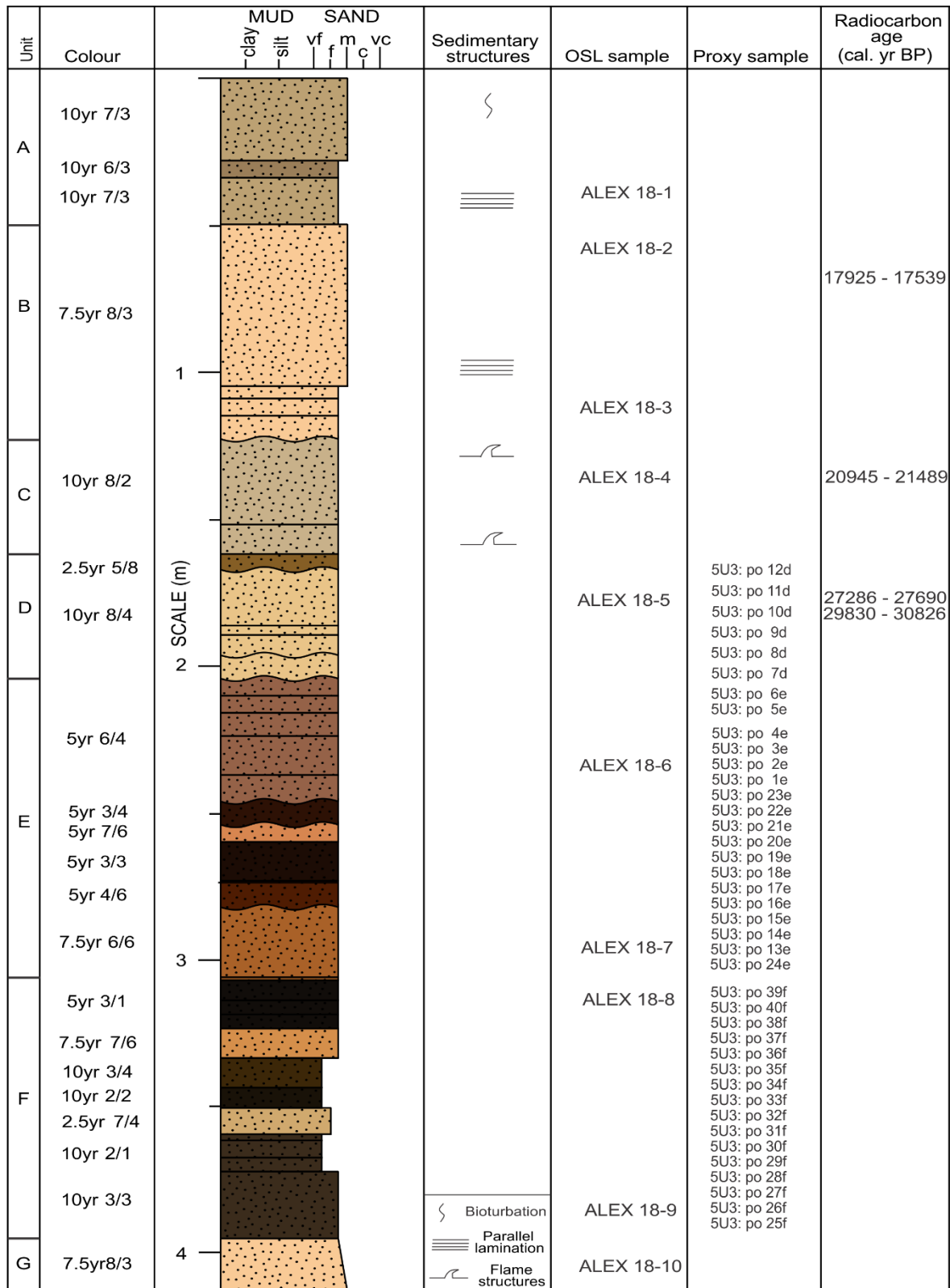


Figure 4. Stratigraphic log of the sedimentary sequence at Alexandra Cave. The sequence is classified into seven distinct units A-G. Sediment colours are from the Munsell Soil Colour Chart. The sequence consists of fine to medium sand with sedimentological structures. OSL and proxy sample locations are shown alongside the stratigraphic log. Calendrical ages produced by radiocarbon dating of charcoal have been calibrated with OxCal using the SHCal13 dataset, and are adapted from McCluskey (2012).

## Geochronology

To determine appropriate preheat temperatures for  $D_e$  determination, an OSL dose recovery test of ALEX 18-5 was conducted on multi-grain aliquots using various test-dose preheat temperatures ranging from 160°C for 10 seconds (s) to 220°C for 10 s. A regenerative preheat temperature of 260°C for 10 s and a test dose preheat of either 220°C for 10 s or 200°C for 10 s yielded the closest estimates of the given dose of 45.2 Gy (Figure 5).

The suitability of these chosen conditions were further tested with a single-grain dose recovery test for 300 grains of ALEX 18-1, ALEX 18-5 and ALEX 18-10 using test dose preheats of 200°C for 10 s and 220°C for 10 s. Successful dose recoveries were obtained using a test-dose preheat of 220°C for 10 s, with weighted mean measured-to-given ratios of  $0.99 \pm 0.02$ ,  $0.94 \pm 0.04$  and  $0.93 \pm 0.04$  (Table 2). The single-grain  $D_e$  values of each sample were subsequently measured with preheat temperature of 260°C for 10 s and a test-dose of 220°C for 10 s following the outcome of these suitability analyses.

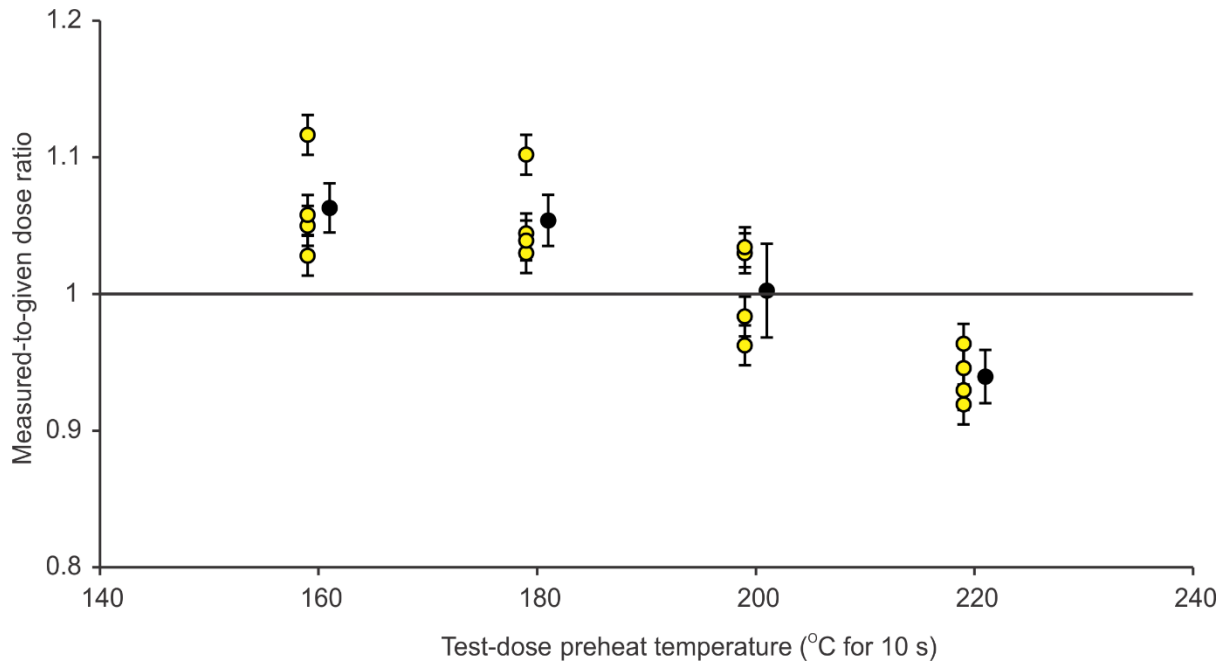


Figure 5. Multi-grain dose recovery test performed using varying test-dose preheat temperatures of 160 – 220°C (each held for 10 s). Four multi-grain disks containing several hundred quartz grains were measured for each preheat temperature (yellow circles). The weighted mean measured-to-given dose ratios (black circles) are also shown for test-dose preheat conditions of 160 – 220°C (for 10 s each). The given dose for each disc was  $45.2 \pm 0.9$  Gy. All dose values are shown with their  $\pm 2\sigma$  uncertainties.

Table 2. Single-grain dose recovery test for samples ALEX 18-1, ALEX 18-5 and ALEX 18-10 using a regenerative preheat temperature of 260°C for 10 s and a test-dose preheat temperature of either 200°C for 10 s or 220°C for 10 s. The dose values are shown with their  $\pm 1\sigma$  uncertainties.

| Single - grain dose recovery test |   |                     |                     |                 |                     |                             |
|-----------------------------------|---|---------------------|---------------------|-----------------|---------------------|-----------------------------|
| Sample                            | Test-dose preheat temperature (°C for 10 s) | No. grains measured | No. grains accepted | Given dose (Gy) | Recovered dose (Gy) | Measure-to-given dose ratio |
| ALEX 18-1                         | 200   | 300                 | 80                  | 30.6 $\pm$ 0.6  | 33.0 $\pm$ 0.8      | 1.07 $\pm$ 0.02             |
| ALEX 18-5                         | 200   | 300                 | 75                  | 61.0 $\pm$ 1.2  | 62.3 $\pm$ 1.5      | 0.99 $\pm$ 0.02             |
| ALEX 18-10                        | 200   | 300                 | 62                  | 91.8 $\pm$ 3.6  | 72.6 $\pm$ 2.4      | 0.80 $\pm$ 0.02             |
| ALEX 18-1                         | 220   | 300                 | 80                  | 30.6 $\pm$ 0.6  | 30.3 $\pm$ 1.2      | 0.99 $\pm$ 0.02             |
| ALEX 18-5                         | 220   | 300                 | 75                  | 61.0 $\pm$ 1.2  | 57.9 $\pm$ 2.6      | 0.94 $\pm$ 0.04             |
| ALEX 18-10                        | 220   | 300                 | 62                  | 91.8 $\pm$ 3.6  | 85.7 $\pm$ 4.8      | 0.93 $\pm$ 0.04             |

The single-grain  $D_e$  distributions cover a very broad range of 7.5 – 92 Gy for the combined dataset (Figure 6a – b). The  $D_e$  values are continuous and in stratigraphic order, within error, throughout the sequence, with the exception of ALEX 18-9 (92.1  $\pm$  2.5 Gy) and ALEX 18-10 (75.9  $\pm$  2.9 Gy) (Table 3). The overdispersion parameter, which indicates the amount of scatter in each  $D_e$  distribution above and beyond the empirical  $D_e$  uncertainties, ranges from 20% to 31%. Samples with overdispersion values of 20 – 25% were considered to be in the normal range for well-bleached, undisturbed samples (Arnold & Roberts, 2009) and their final  $D_e$  value was therefore derived using a Central Age Model (CAM). Samples with overdispersion values above 25% (ALEX 18-1, ALEX 18-2, ALEX 18-4 and ALEX 18-5) were considered to exhibit more significant  $D_e$  scatter related to their depositional history, and were fitted with a three parameter Minimum Age Model (MAM), with the exception of ALEX 18-10, where the MAM was not statistically justified over the CAM on the basis of its inferior maximum likelihood values (Arnold & Roberts, 2009; Galbraith & Roberts, 2012). ALEX 18-8 and ALEX 18-9 have proportionately higher present-day water contents of 12 –

14% (Table 3). ALEX 18-9 and ALEX 18-10 have higher beta (0.36 – 0.43 Gy/ka) and gamma (0.29 – 0.34 Gy/ka) dose rates (Table 3).

The sedimentary sequence is constrained from 17.7 to 106.3 ka, spanning four MIS stages (Figure 7). ALEX 18-1 to ALEX 18-4 correspond to the Last Glacial Maximum; ALEX 18-5 and ALEX 18-6 span MIS 3; ALEX 18-7 and ALEX 18-8 correlate to MIS 4; and ALEX 18-9 and ALEX 18-10 span MIS 5 (Figure 7). Sedimentation rates were lowest during interglacial periods (MIS 3 and 5), with MIS 5 observing lowest sedimentation rate of 2.96 cm/ka. Higher sedimentation rates were observed during the glacial periods (MIS 2 and 4), with highest sedimentation rate occurring during MIS 2, at 9.42 cm/ka (Table 4).

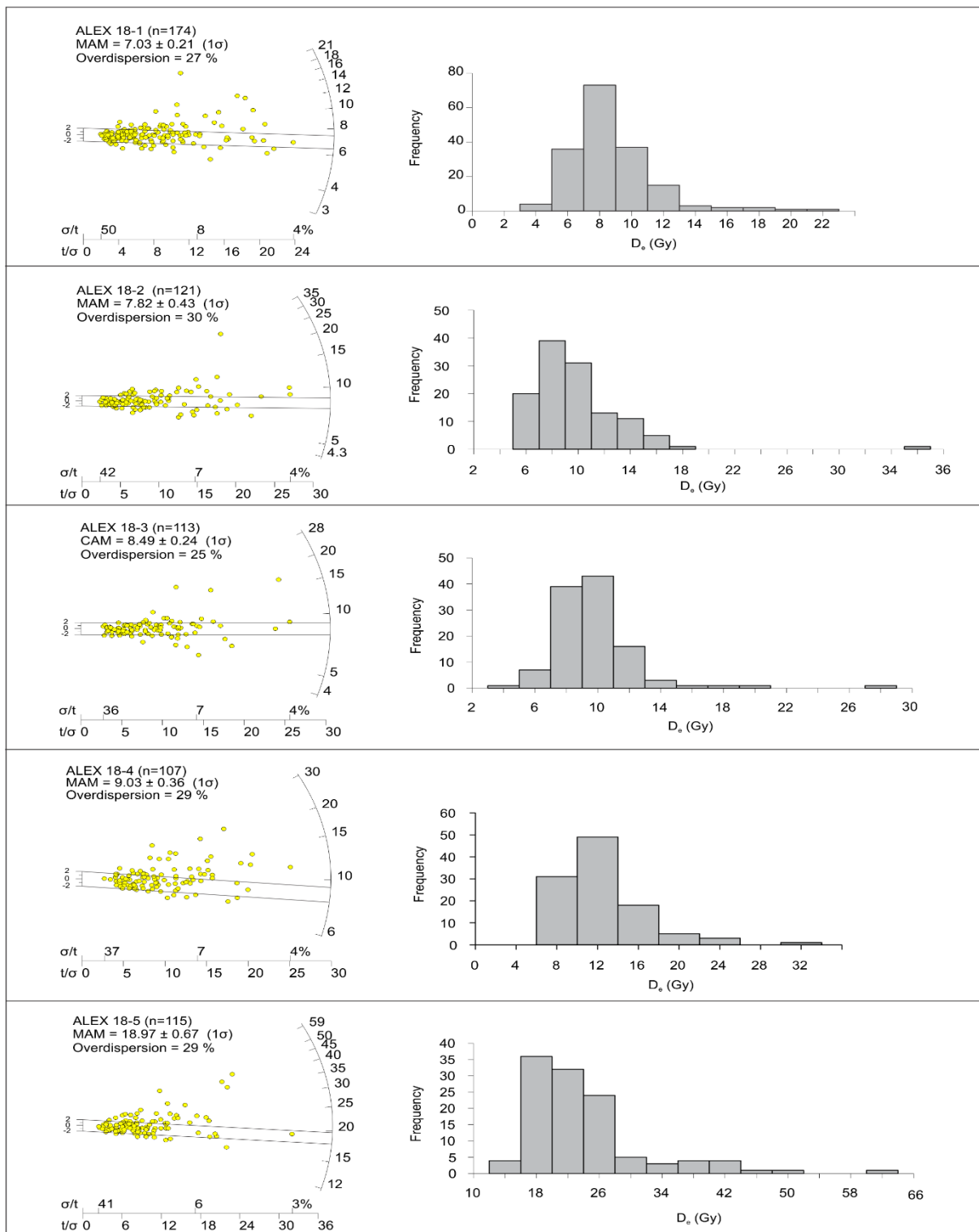


Figure 6a. Radial plot and histograms of equivalent dose rates ( $D_e$ ) measured for OSL samples ALEX 18-1 to ALEX 18-5. 500 individual grains were measured per sample, of which only grains that passed the SAR quality assurance criteria (Appendix 5) are plotted in this figure. Sample sizes range from 107 – 174 grains. A 3-parameter minimum age model (Galbraith et al., 1999) is used to derive the final  $D_e$  of samples ALEX 18-1, 2, 4 and 5, while the weighted mean  $D_e$  value (calculated using the central age model) was used for all other samples.

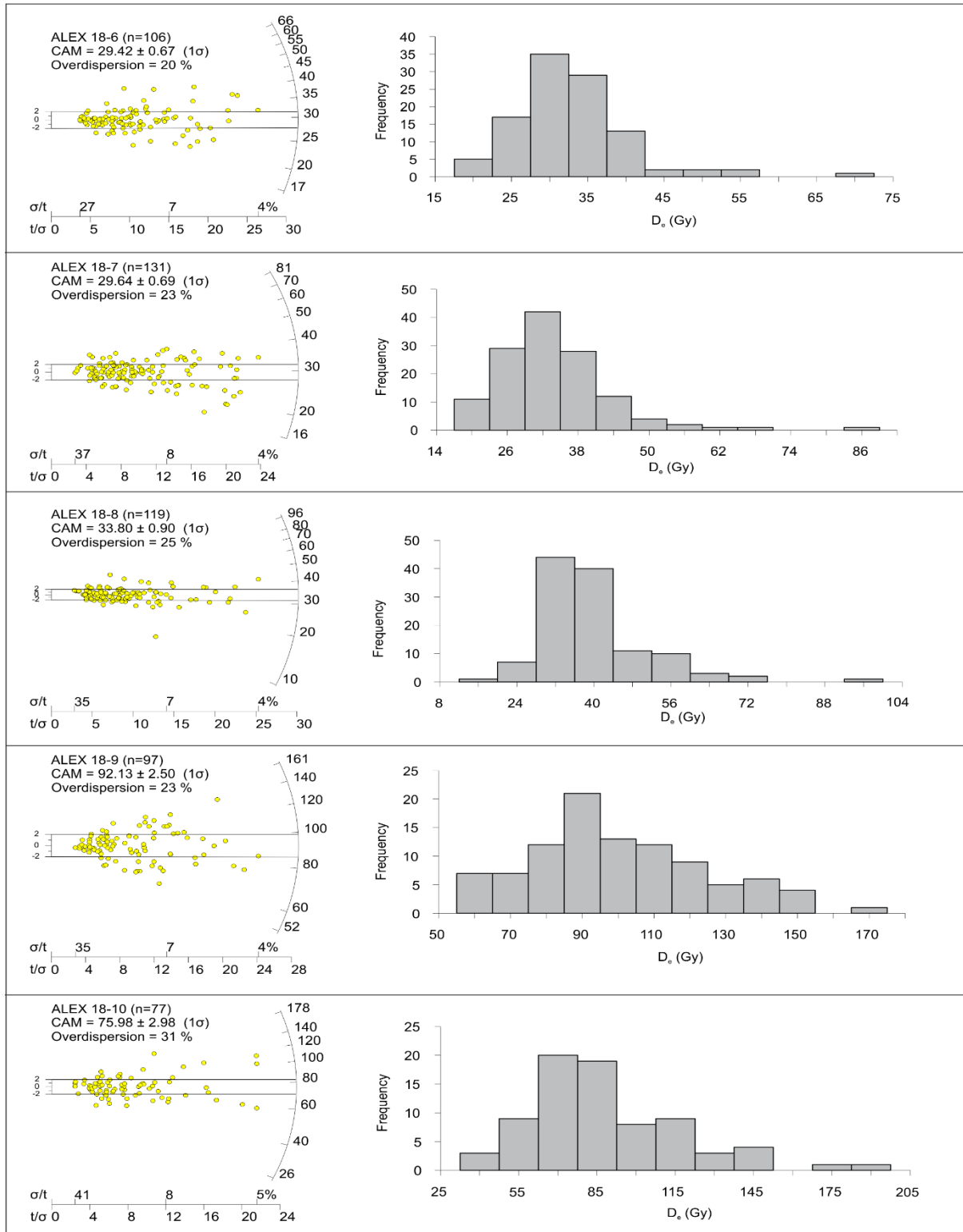


Figure 6b. Radial plot and histogram of  $D_e$  measured from ALEX 18-6 to ALEX 18-10 with central age model. 500 individual grains were measured, of which only grains that pass the selection criteria (Appendix 5) are plotted in this figure. Sample sizes range from 77 – 131 grains. A minimum age model was not applied to ALEX 18-10 despite the large overdispersion value ( $> 25\%$ ) because the maximum likelihood score of MAM was similar to that of the CAM.

Table 3. Summary statistics of radionuclide concentrations, environmental dose rate,  $D_e$  measurements and final OSL ages for the Alexandra Cave samples. Field water content is expressed as percentage of dry mass mineral fraction with  $\pm 10\%$  uncertainty. \*Water content for ALEX18-10 is corrected for 50% saturation. Gamma dose rates were calculated from in situ measurements made at each sampling position using a NaI detector. Beta dose rates were calculated using a Risø GM-25-5 low-level beta counter. Individual radionuclide concentrations were derived from the field gamma spectra using the ‘energy windows’ method from Arnold et al., (2012). Cosmic dose rates were calculated by taking into account the geomagnetic latitude, altitude and thickness of overburden (Prescott & Hutton, 1994). The total dose rate includes an internal dose rate of 0.03 Gy/ka with an uncertainty of 30% (Bowler et al., 2003). Final OSL ages were calculated as mean  $\pm$  total uncertainty at 68% confidence interval.

| Sample     | Depth (cm) | Water content   | Radionuclide concentrations |                         |                     | Environmental dose rate (Gy/ka) |                 |                      | Total dose rate (Gy/ka) | $D_e$ (Gy)       | Age Model | Final Age (ka)    |
|------------|------------|-----------------|-----------------------------|-------------------------|---------------------|---------------------------------|-----------------|----------------------|-------------------------|------------------|-----------|-------------------|
|            |            |                 | $^{238}\text{U}$ (ppm)      | $^{228}\text{Th}$ (ppm) | $^{40}\text{K}$ (%) | Gamma dose rate                 | Beta dose rate  | Cosmic-ray dose rate |                         |                  |           |                   |
| ALEX 18-1  | 37         | 1.8 $\pm$ 0.1   | 0.47 $\pm$ 0.05             | 1.34 $\pm$ 0.11         | 0.12 $\pm$ 0.01     | 0.15 $\pm$ 0.01                 | 0.14 $\pm$ 0.01 | 0.08 $\pm$ 0.01      | 0.40 $\pm$ 0.02         | 7.73 $\pm$ 0.19  | MAM       | 17.69 $\pm$ 1.16  |
| ALEX 18-2  | 60         | 2.1 $\pm$ 0.2   | 0.47 $\pm$ 0.05             | 1.58 $\pm$ 0.12         | 0.13 $\pm$ 0.01     | 0.16 $\pm$ 0.01                 | 0.17 $\pm$ 0.01 | 0.08 $\pm$ 0.01      | 0.44 $\pm$ 0.02         | 8.48 $\pm$ 0.26  | MAM       | 17.75 $\pm$ 1.39  |
| ALEX 18-3  | 94         | 2.4 $\pm$ 0.2   | 0.43 $\pm$ 0.05             | 1.15 $\pm$ 0.10         | 0.12 $\pm$ 0.01     | 0.13 $\pm$ 0.01                 | 0.16 $\pm$ 0.01 | 0.08 $\pm$ 0.01      | 0.41 $\pm$ 0.02         | 8.49 $\pm$ 0.24  | CAM       | 20.93 $\pm$ 1.35  |
| ALEX 18-4  | 120        | 1.7 $\pm$ 0.2   | 0.41 $\pm$ 0.05             | 1.24 $\pm$ 0.10         | 0.12 $\pm$ 0.01     | 0.14 $\pm$ 0.01                 | 0.13 $\pm$ 0.01 | 0.08 $\pm$ 0.01      | 0.40 $\pm$ 0.02         | 9.70 $\pm$ 0.30  | MAM       | 23.99 $\pm$ 1.71  |
| ALEX 18-5  | 172        | 3.9 $\pm$ 0.4   | 0.39 $\pm$ 0.05             | 1.78 $\pm$ 0.14         | 0.23 $\pm$ 0.01     | 0.19 $\pm$ 0.01                 | 0.18 $\pm$ 0.01 | 0.07 $\pm$ 0.01      | 0.47 $\pm$ 0.02         | 21.02 $\pm$ 0.63 | MAM       | 40.57 $\pm$ 2.65  |
| ALEX 18-6  | 214        | 5.3 $\pm$ 0.5   | 0.53 $\pm$ 0.05             | 1.86 $\pm$ 0.13         | 0.24 $\pm$ 0.01     | 0.21 $\pm$ 0.01                 | 0.25 $\pm$ 0.01 | 0.07 $\pm$ 0.01      | 0.56 $\pm$ 0.03         | 29.42 $\pm$ 0.67 | CAM       | 52.15 $\pm$ 2.96  |
| ALEX 18-7  | 285        | 4.2 $\pm$ 0.4   | 0.42 $\pm$ 0.05             | 1.70 $\pm$ 0.12         | 0.16 $\pm$ 0.01     | 0.17 $\pm$ 0.01                 | 0.16 $\pm$ 0.01 | 0.08 $\pm$ 0.01      | 0.44 $\pm$ 0.02         | 29.64 $\pm$ 0.69 | CAM       | 67.11 $\pm$ 4.00  |
| ALEX 18-8  | 325        | 13.0 $\pm$ 1.3  | 0.57 $\pm$ 0.06             | 2.03 $\pm$ 0.15         | 0.27 $\pm$ 0.01     | 0.23 $\pm$ 0.01                 | 0.24 $\pm$ 0.01 | 0.08 $\pm$ 0.01      | 0.57 $\pm$ 0.03         | 33.80 $\pm$ 0.90 | CAM       | 59.03 $\pm$ 3.53  |
| ALEX 18-9  | 374        | 14.4 $\pm$ 1.4  | 0.66 $\pm$ 0.07             | 3.79 $\pm$ 0.24         | 0.33 $\pm$ 0.02     | 0.34 $\pm$ 0.02                 | 0.43 $\pm$ 0.02 | 0.07 $\pm$ 0.01      | 0.86 $\pm$ 0.04         | 92.13 $\pm$ 2.50 | CAM       | 107.31 $\pm$ 6.33 |
| ALEX 18-10 | 392        | 11.2 $\pm$ 1.1* | 0.61 $\pm$ 0.07             | 3.36 $\pm$ 0.22         | 0.29 $\pm$ 0.02     | 0.29 $\pm$ 0.01                 | 0.36 $\pm$ 0.02 | 0.06 $\pm$ 0.01      | 0.72 $\pm$ 0.04         | 75.98 $\pm$ 2.98 | CAM       | 106.34 $\pm$ 6.96 |



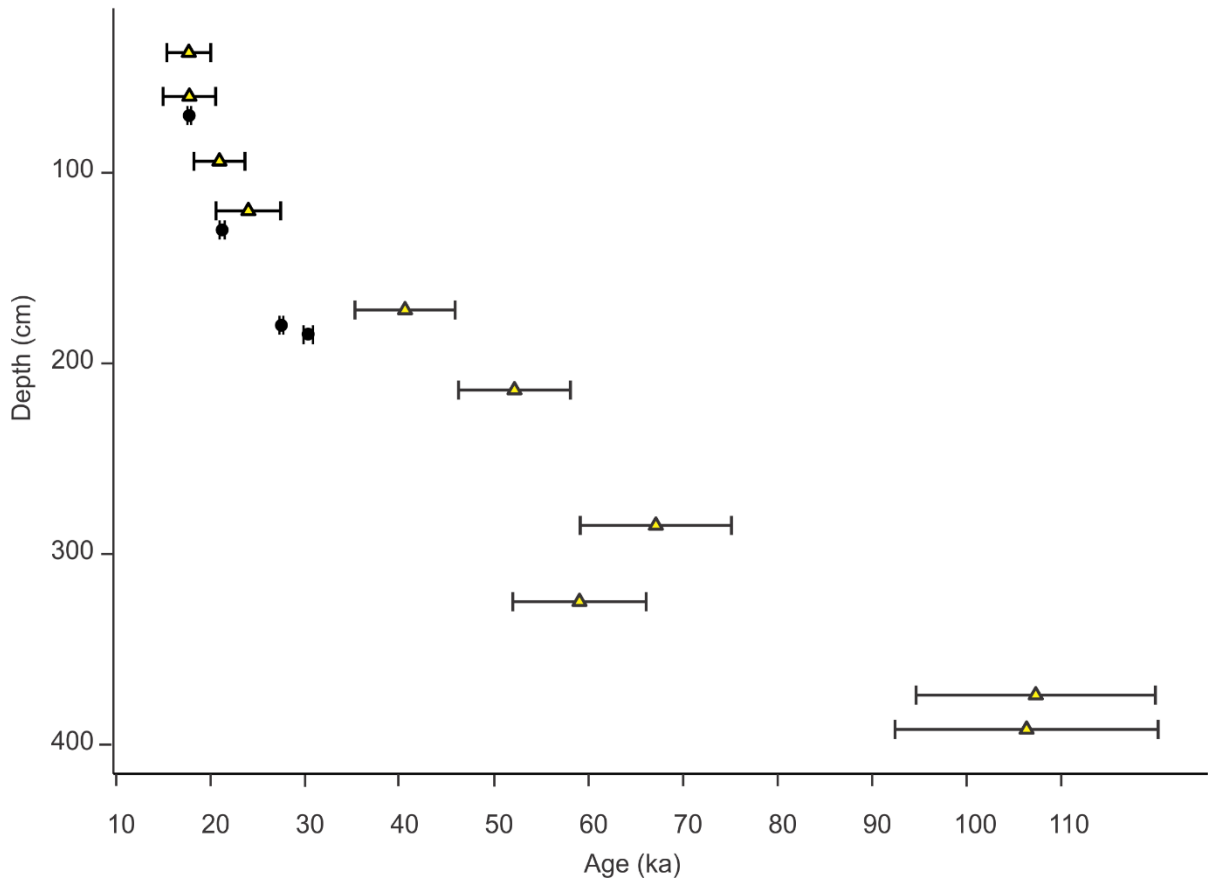


Figure 7. Age-depth profile of Alexandra Cave sequence. OSL ages are plotted with their  $\pm 2\sigma$  ranges (yellow triangles). Radiocarbon calendar ages (calibrated 95.4% CI ranges) are plotted as black dots and have been calibrated in OxCal using SHCal13. The lowermost two  $^{14}\text{C}$  ages are considered minimum age estimations according to the interpretations of McCluskey (2012).

Table 4. Sedimentation rate of Alexandra Cave sediments. The Bayesian age-depth model used to reconstruct accumulation history statistics for these deposits is based on the OSL ages and sample depth information, and has been constructed using the ‘Bacon’ package in R. The model ran 17,820,000 Markov Chain Monte Carlo (MCMC) iterations to estimate mean ages down the sequence. The estimated starting date of sediment accumulation was set to be 15 ka. 90% of OSL ages lie within the age-depth model’s 95% CI range. Marine Isotope Stages are classified according to Lisiecki and Raymo (2005).

| Samples                 | Depth (cm) | Age constrain | MIS | Sedimentation rate (cm/ka) |
|-------------------------|------------|---------------|-----|----------------------------|
| ALEX 18-9 to ALEX 18-10 | 327 – 392  | 71098 – 93071 | 5   | 2.96                       |
| ALEX 18-7 to ALEX 18-8  | 252 – 326  | 57111 – 70851 | 4   | 5.38                       |
| ALEX 18-5 to ALEX 18-6  | 132 – 251  | 29398 – 56913 | 3   | 4.32                       |
| ALEX 18-1 to ALEX 18-4  | 1 – 131    | 15345 – 29145 | 2   | 9.42                       |

## Charcoal

The micro-charcoal record shows a distinct peak centred on 353 cm depth (56.75 particles/cm<sup>3</sup>), a smaller peak at 222 cm (21.75 particles/cm<sup>3</sup>) and, although not fully characterised by more data points, a broad peak from 0 – 190 cm (22.25 particles/cm<sup>3</sup>) (Figure 8). The macro-charcoal fraction has four peaks at 357 cm (9.01 mm<sup>-2</sup> cm<sup>3</sup>), 315 cm, (5.43 mm<sup>-2</sup> cm<sup>3</sup>), 264 cm (7.36 mm<sup>-2</sup> cm<sup>3</sup>) and 164 cm (11.14 mm<sup>-2</sup> cm<sup>3</sup>) depths. The macro-charcoal record reveals that local fires are very low in intensity at 0 – 120cm (0.38 – 1.83 mm<sup>-2</sup> cm<sup>3</sup>). Macro- and micro-charcoal counts for each sample are presented in Appendix 10.

To assess the relationship between micro- and macro-charcoal, an untransformed linear regression was performed. An  $r^2$  correlation coefficient of 0.03 (Figure 9) indicates that the two fractions are very weakly correlated, and can be interpreted independently to represent regional and local fire respectively.

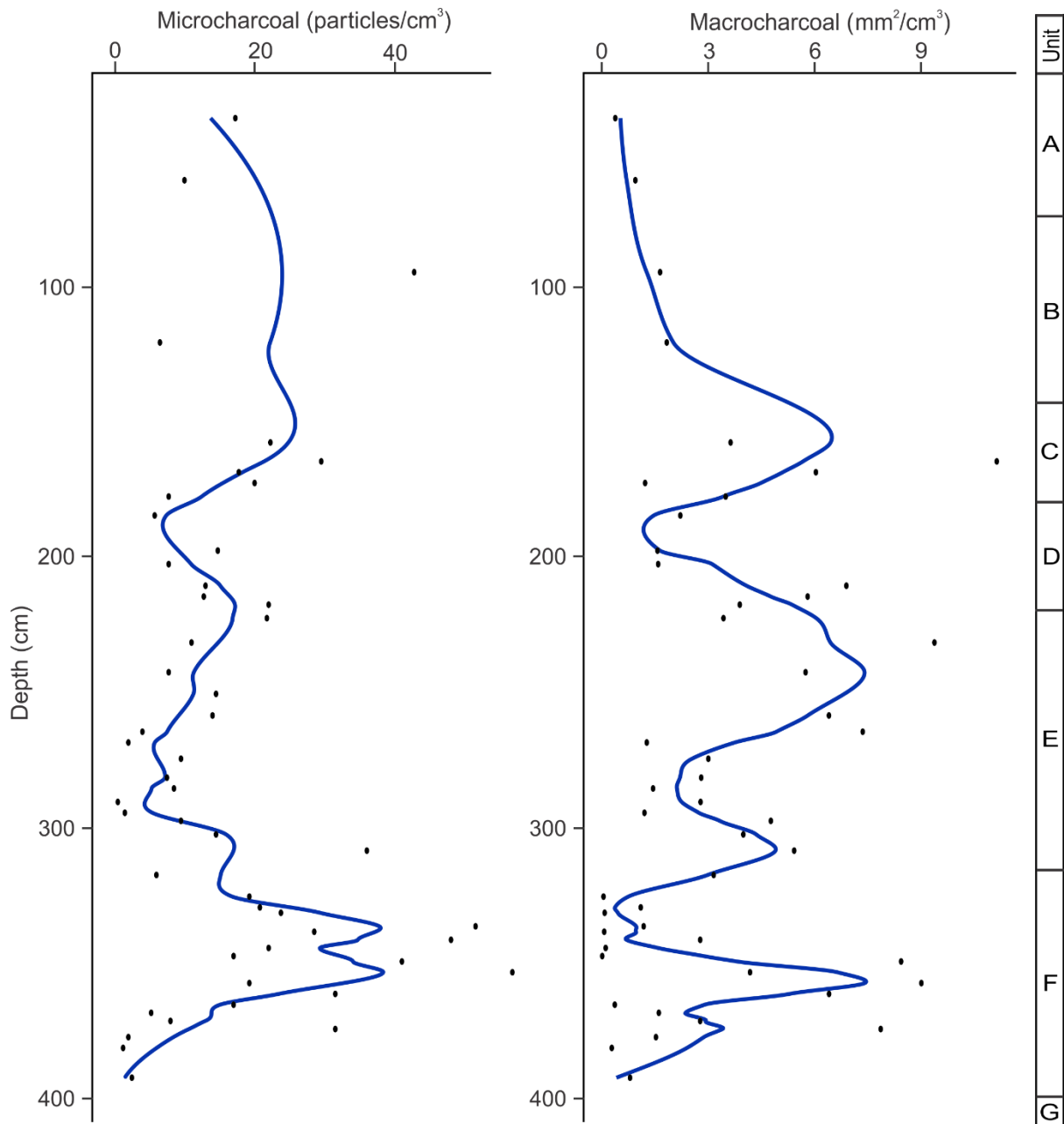


Figure 8. Micro- and macro-charcoal counts as a function of depth through the Alexandra Cave sedimentary sequence. An outlier was removed from the macro-charcoal dataset (value 25.1 mm<sup>2</sup> per cm<sup>3</sup> at 250 cm). Black dots on the left- and right-hand plots represent 50 and 49 individual data points respectively. A 0.2 LOESS smoothing spline has been fitted through each dataset, represented by the blue line.

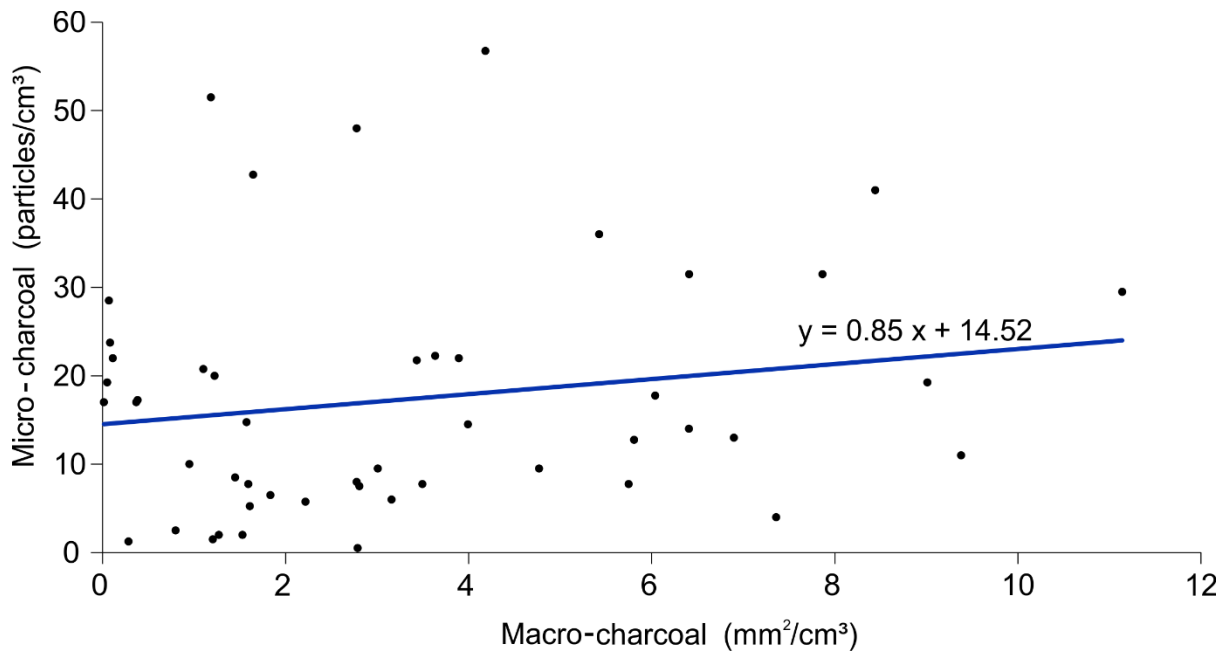


Figure 9. Untransformed linear regression of micro-charcoal (<100  $\mu\text{m}$ ) against macro-charcoal (>250  $\mu\text{m}$ ) concentrations. There is no significant correlation,  $r^2 = 0.032$  at 0.05  $\alpha$  (Degrees of Freedom = 1, F-statistic = 1.52, p-value = 0.00013 (threshold p-value: <0.05)).

### **Pollen & *Sporormiella***

No pollen or *Sporormiella* spores were observed in any of the 50 samples. The lycopodium spike introduced during the sample preparation was observed in the final fraction, indicating that the lack of fossil pollen and *Sporormiella* was not related to experimental procedures, but appears to reflect genuine absence.

### Carbon isotopes

The charcoal pieces range in carbon isotope ratio between -18.43‰ (37 cm) and -28.58‰ (392 cm). Bulk  $\delta^{13}\text{C}$  were mostly within the  $\pm 2\sigma$  range of individual charcoal pieces, with the exception of samples at 285 cm and 35 cm. The bulk  $\delta^{13}\text{C}$  show peak values of -22.31‰ at 285 cm and -23.85‰ at 60 cm depth (Figure 10). A table of all  $\delta^{13}\text{C}$  values is available in Appendix 11. Individual charcoal pieces were imaged but could not be identified with confidence for classification of plant type.

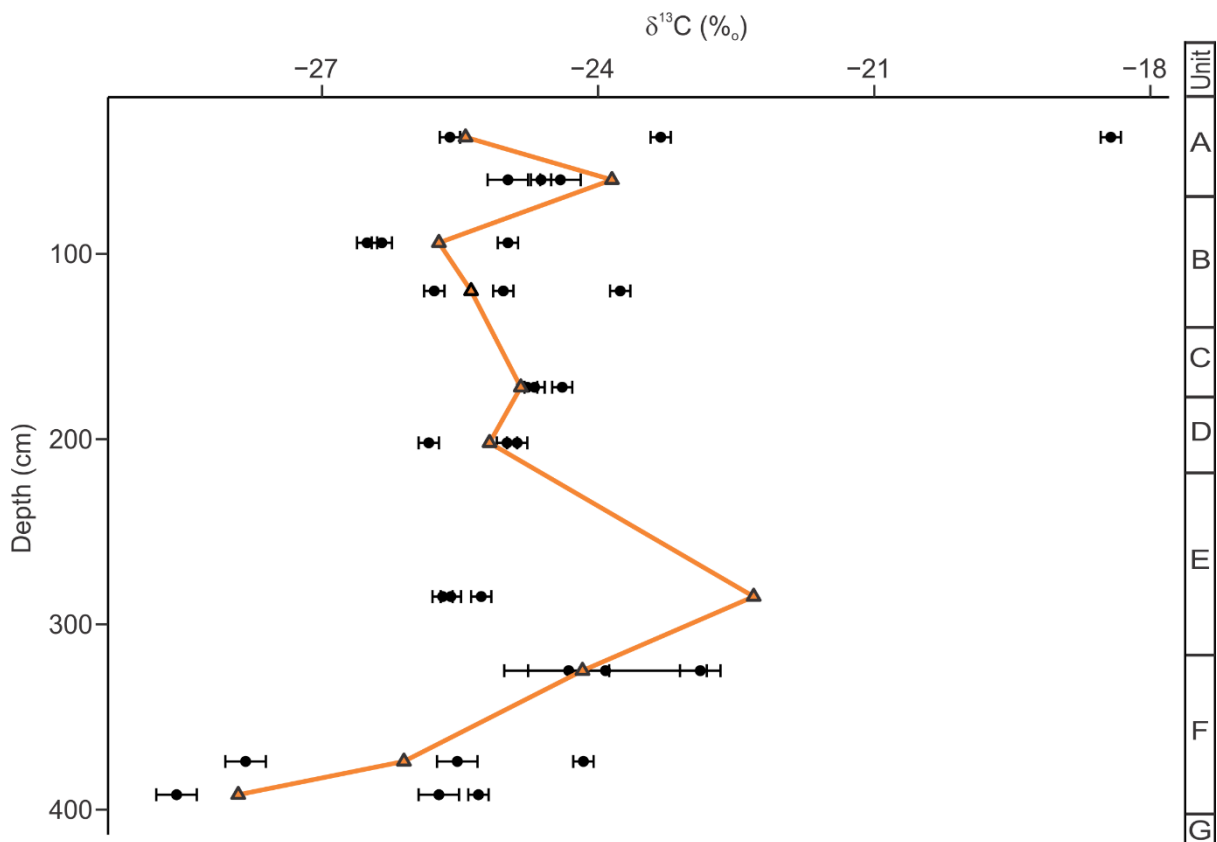


Figure 10.  $\delta^{13}\text{C}$  isotope ratios (‰) as a function of depth through the stratigraphic profile. Black dots represent three individual charcoal pieces measured from the OSL sample positions of ALEX 18-1 to ALEX 18-10 at  $\pm 2\sigma$ . The orange line represents the bulk carbon isotope data.  $\delta^{13}\text{C}$  is reported in parts per mil relative to the Vienna Pee Dee Belemnite standard (VPDB).

## **Geochemistry**

The ITRAX scanner analysed 17 elements in total, and the key indicator elements selected for this study (see Table 1) are plotted in Figure 11. From the dataset, three phases of elemental change can be observed. From the base of the section upwards, a substantial change is observed across all elements at 300 – 392 cm, which corresponds to Unit F. A three-fold increase was observed in Ca, K, Fe, P and inc/coh ratios, while a 2.5 fold decrease was observed for S, Al and Si. The middle section, 119 – 299 cm spanning Units E to C, is generally stable for all elements, with no major fluctuations. Towards the top of the core (0 – 120 cm), a slight increase in Si/Ti ratio (1 – 2) and decrease in inc/coh ratio (1.39 – 1.31) is observed in Units B and A.

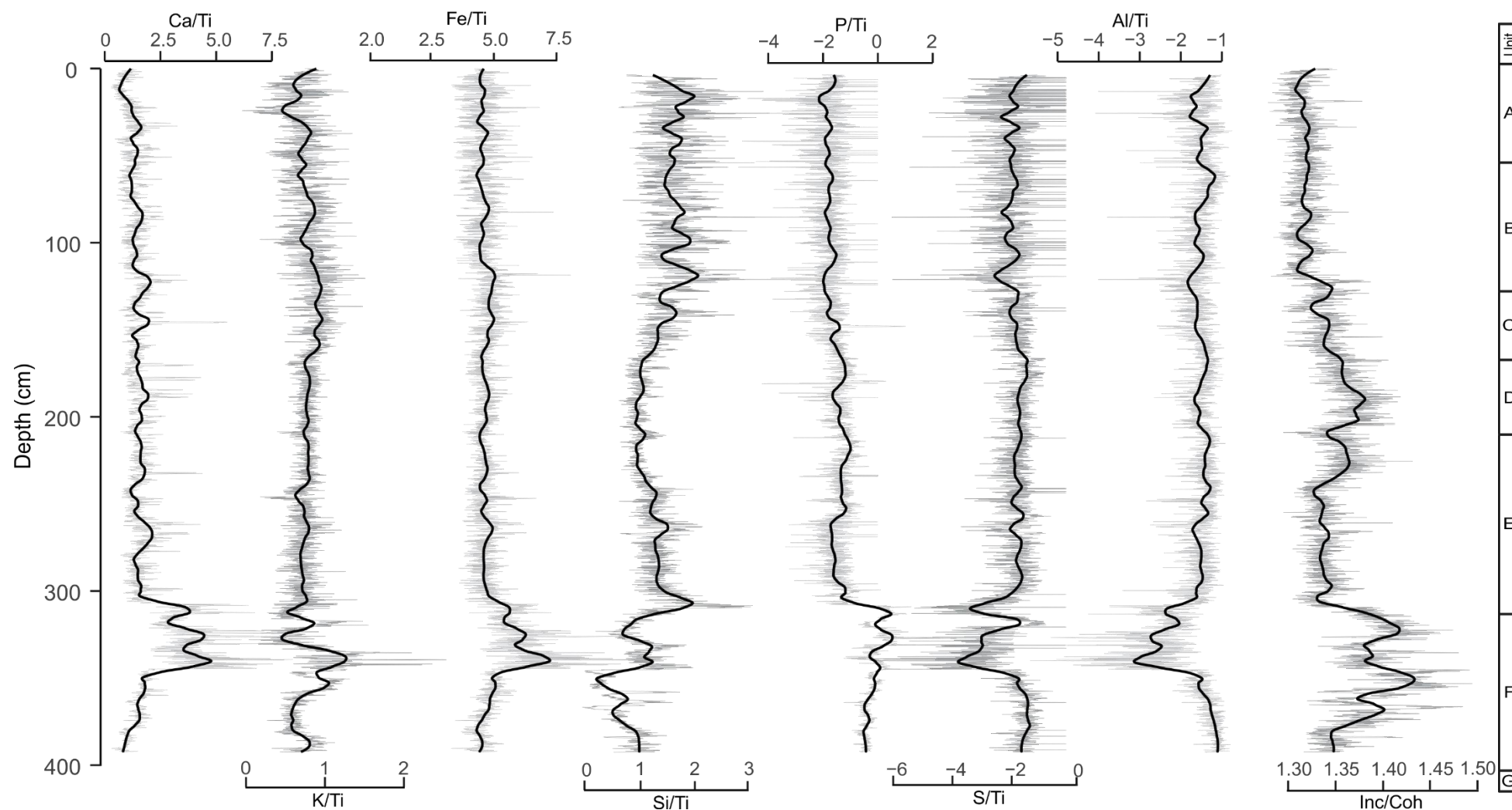


Figure 11. Ratio of selected indicator elements measured by the ITRAX core scanner. The ‘inc/coh’ ratio refers to coherent and incoherent scatter values XRF counts have been centered log-ratio transformed and normalised against Ti. Raw data is plotted in grey with a 0.05 LOESS smoothing spline in black, performed in R v 3.5.0. Elements were selected based on past geochemical studies conducted in NCNP and other XRF studies in similar contexts around the world (Burnett et al., 2011; Croudace & Rothwell, 2015; Forbes & Bestland, 2007; Guyard et al., 2007; Jouve et al., 2013).

## DISCUSSION

### Geochronology

The sedimentary sequence in Alexandra Cave covers critical timeframes from MIS 5 to MIS 2, and overlaps with the megafauna extinction window (Figure 12). The final OSL ages in Alexandra Cave are stratigraphically consistent within error (Table 3). The suitability of the OSL ages is also supported by their consistency with the two reliable radiocarbon ages produced by McCluskey (2012) for Units B – C. Interestingly, there is a systematic divergence of up to 10 ka for the OSL ages and the minimum radiocarbon ages obtained on Units D (Figure 7). This divergence confirms the original interpretation of McCluskey (2012) that the two lowermost radiocarbon ages should be treated with caution due to degradation of the charcoal samples (McCluskey, 2012). Archaeological sites are prone to charcoal degradation as a result of chemical alteration and physical translocation, and such degraded specimens typically have lower carbon content compared to unaltered samples, which can result in underestimation of ages (Bird et al., 2002; Cohen-Ofri et al., 2006). The application of single-grain OSL has extended the existing chronology of the Alexandra Cave sediment sequence, and provided an independent means of assessing the veracity of available  $^{14}\text{C}$  age control at the site.

A critical assumption of OSL dating is that the light sensitive OSL traps were completely empty at the time of burial. If the grains are not sufficiently bleached, a residual signal will be retained, and calculated ages will be an overestimation of the true depositional age (Aitken, 1985). Partially bleached grain populations are observed in the single-grain  $D_e$  datasets of ALEX 18-1, ALEX 18-2, ALEX 18-4 and ALEX 18-5 and suggests an input of grains near cave entrances not being fully reset, that were subsequently washed into its present-day



sampling position along with well-bleached grains (Arnold et al., in prep, 2018). Partial bleaching was similarly observed for quartz grains in Victoria Fossil Cave, where OSL ages had a wide  $D_e$  distribution and high overdispersion values of 35 – 44% (Macken et al., 2011). The present study therefore confirms the importance of undertaking single-grain OSL dating in combination with statistical analysis of  $D_e$  datasets (minimum age modelling) to derive reliable ages in Alexandra Cave.

A second assumption of OSL dating is that the sediment has not undergone post-depositional mixing and the sediment dose rate has not changed over time (Roberts et al., 2015). OSL ages from Blanche Cave were consistently older than radiocarbon ages of the same units and were interpreted to be a result of dose rate disequilibrium (Darrénougué et al., 2009). Dose rate disequilibrium or beta dose rate heterogeneity could partly explain the high overdispersion of 31% in ALEX 18-10 (Figure 6b); Overdispersion values were >20% and the minimum age model was not favoured over the central age model on statistical grounds (Galbraith & Roberts, 2012). Such systematic dose rate effects could be better resolved by undertaking comparative luminescence dating measurements using the post-infrared infrared stimulated luminescence (pIR-IRSL) signal of K-feldspar grains from ALEX 18-10 (Huntley & Lamothe, 2001).

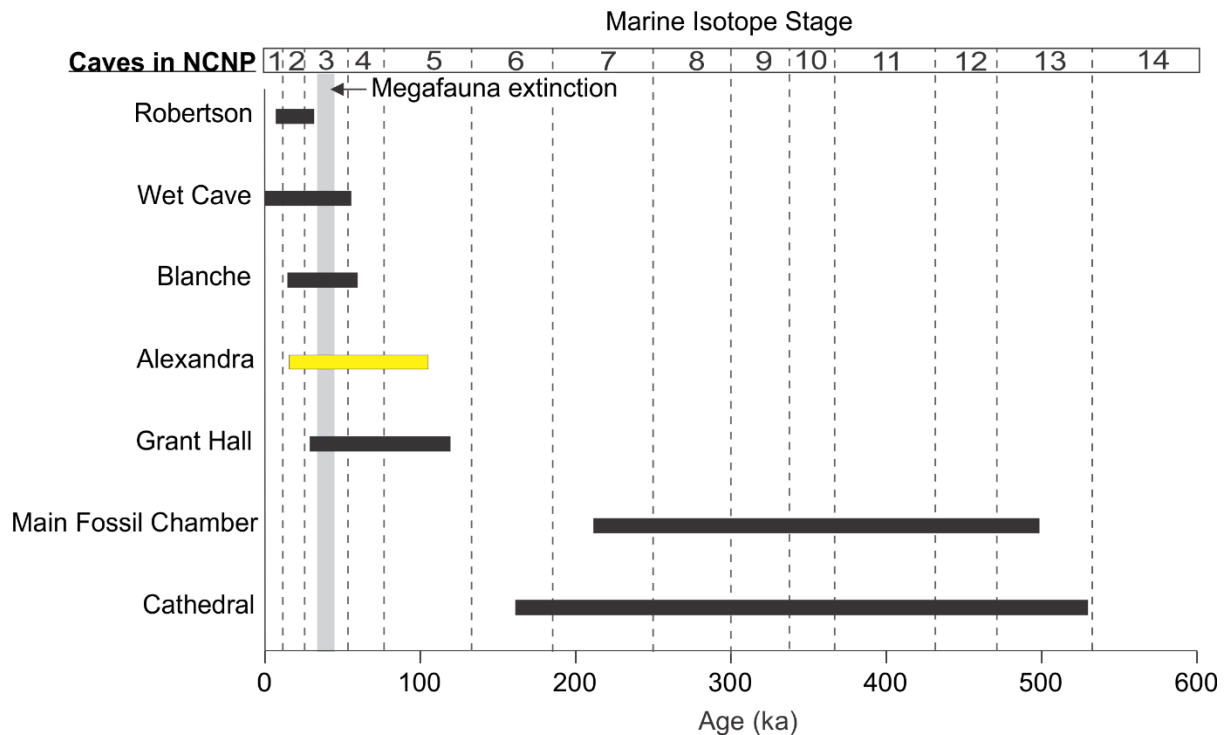


Figure 12. Alexandra Cave chronology in the context of surrounding caves in Naracoorte Caves National Park. Robertson, Wet Cave, Blanche, Grant Hall, Main Fossil Chamber and Cathedral Cave have sediment sources that have been dated through Radiocarbon, OSL or U-series dating (Grün et al., 2001; Prideaux et al., 2007; Darrénougué et al., 2009; Macken et al., 2012; St Pierre et al., 2012; Macken et al., 2013).

### Fire history

The sedimentological interpretations suggest that charcoal was likely washed into Alexandra Cave from the surrounding land surface, particularly as some of the charcoal bands observed in the sequence were horizontal. Macro-charcoal demonstrated frequent episodes of local fire from MIS 5 – 3 (392 to 160 cm), after which fire occurrence dropped to near zero in MIS 2 (Figure 8). Two striking increases in the micro-charcoal concentrations occur at 85 – 71 ka, with  $\delta^{13}\text{C}$  ratios suggesting increased moisture-stress, and 42 – 35 ka, with no corresponding change in moisture-stress (Figure 13). No correlation was observed between the charcoal trends and sedimentation rates in the cave. Similarly, no relationship was deduced with the collective Australasian charcoal datasets (223 records) by Mooney et al. (2011) (Figure 13). It

is plausible that this is a result of the charcoal in Alexandra Cave representing fire frequencies in a more localised setting compared to continental-scale trends.

### **Palaeovegetation**

The  $\delta^{13}\text{C}$  trends may be interpreted as an indicator of moisture availability in the external environment of Alexandra Cave. Most of the  $\delta^{13}\text{C}$  values were within the  $\text{C}_3$  plant range, with the exception of an individual piece from 37 cm depth, which had a  $\delta^{13}\text{C}$  value of  $-18.43\text{‰}$  ( $\text{C}_4$  species range) (Turney, 2012); the bulk value at this depth also tends toward  $\text{C}_4$  species range ( $-25.44\text{‰}$ ), suggesting that this individual piece might be a true reflection of the moisture in the environment, rather than an outlier. ALEX 18-1 and ALEX 18-7 have bulk values that lie outside the range of individual charcoal pieces (Figure 10), indicating some variability in the fire regime that was not fully captured by the three individually analysed charcoal fragments picked from this level. Alternatively, the bulk sample could be from a different source to the individual pieces picked.

The isotopic signature of charcoal may have also partly varied due to changes in temperature, duration of fire and vegetation type, in addition to moisture availability in the environment (Turney, 1999). There has been contradictory evidence on the extent of carbon isotopic alteration during the carbonisation of wood related to fire temperature variability. A depletion in  $\delta^{13}\text{C}$  of 1 – 1.4% was observed at fire temperatures ranging 150 – 180<sup>0</sup>C (Czimczik et al., 2002; Schleser et al., 1991; Turney et al., 2006). The findings of Turekian et al. (1998) contradict these findings, noting an enrichment in  $\delta^{13}\text{C}$  of 0.5‰ in burned material. Given these complex and variable results, the effects of carbonisation on  $\delta^{13}\text{C}$  values have not been taken into account in this study.

It should be noted that the resolution of this dataset is low, with only 10 samples analysed for the entire 4 meters. Ideally, either more individual pieces, or higher resolution bulk sampling would be needed to better quantify the apparent trends. Nevertheless, the existing data still provides a useful proxy for the extent of physiological stress on C<sub>3</sub> plants from moisture availability, as most of the individual charcoal values lie within the range of the bulk  $\delta^{13}\text{C}$ .

The absence of pollen in Alexandra Cave was unexpected, given that Blanche Cave, located only 400 m away, has 29 pollen taxa identified (Darrénougué et al., 2009). Pollen preservation in caves can be affected by proximity to cave openings, changing conditions within the cave or mode of transport (Hunt & Fiacconi, 2018). Taking into account the closed nature of Alexandra Cave, and the fact that pollen was absent over four separate sections of the sediment deposit (i.e. a broad spatial area of the cave interior), pollen transport could be the critical factor that has influenced preservation in Alexandra Cave. If pollen is primarily transported by airfall, the large openings (>10 m wide) in Blanche Cave would have captured more pollen than the narrow entrances of Alexandra Cave. The sandy sedimentary deposits could also have been transported by processes that enhance pollen erosion, or may be associated with environmental conditions that favour the post-depositional oxidation of pollen (Carrión et al., 2009), which could also account for pollen absence in Alexandra Cave.

Similarly, the absence of *Sporormiella* in Alexandra Cave may reflect airborne dispersal patterns, or narrow entrances. Given that Alexandra Cave was likely a pitfall trap for large fauna (Reed & Bourne, 2000), the absence of *Sporormiella* could perhaps suggest a more complex localised dispersion or post-depositional preservation environment within the cave. Spore representation is fairly inconsistent in Australian sites and may be absent where large herbivores are known to be present. This complication has been attributed to the source

strength and transport systems that incorporate spores into sediment (Dodson & Field, 2017).

With only four documented sites of *Sporormiella* in Australia, it was anticipated that the present study might yield negative results. The results obtained in Alexandra Cave, where large fauna were present in and around the cave (Reed & Bourne, 2000), emphasises the need for a more comprehensive study on the usefulness of *Sporormiella* as a proxy, and its relationship to present-day fauna in Australia.

### **Geochemistry**

XRF scanning of Alexandra Cave sediment has provided high-resolution geochemical data on sedimentary dynamics spanning multiple glacial-interglacial stages. The XRF data is consistent across all key indicator elements, with several shared changes detected through the sequence. The increase in P/Ti and Ca/Ti alongside a decrease in S/Ti at 300 cm, matches with observations of black-red sediment observed in field (Figure 3 & 11). Based on sediment colour and grain size, it was initially speculated that bats may have inhabited the cave.

However, the geochemistry is inconsistent with observations of bat guano layers observed in Robertson Cave, which had high S, P, and Ca and low Fe concentrations (Figure 11). The corresponding increase in Fe/Ti in Alexandra Cave could suggest a change in sediment source or post-depositional alteration (Aufgebauer et al., 2012).

The Si/Ti and inc/coh ratios show the most variation down the core (Figure 11). Si/Ti peaks coincide with high sedimentation rates, an observation also observed in an XRF scanning study of Finland lake cores by Shala et al. (2013), which demonstrated that Si/Ti ratio peaks were associated with sand layers and were inferred to be influxes of silt-sized particles. The water content measured from the geochronology samples (Table 3) match up with the

presence of organic matter, as indicated by the inc/coh ratio, suggesting that the latter represents a reliable proxy for inorganic versus organic content in this environment (Guyard et al., 2007; Jouve et al., 2013).

## **Palaeoenvironmental reconstruction and regional associations**

### **Marine Isotope Stage 5 (123 – 71 ka)**

Charcoal and geochemistry data from Alexandra Cave suggests that MIS 5 was wet with frequent fires. The increase in organic matter and decrease in detrital input from inc/coh and Si/Ti ratios observed during 89 and 70 ka (Figure 13), is consistent with speleothem formation records from a series of caves in NCNP, which record a large peak in formation frequency during MIS 5 associated with a period of high precipitation (Ayliffe, 1998). Regionally, high precipitation in MIS 5 might have resulted in abundant vegetation growth that stabilised exposed fossilised dune deposits in south-east Australia (Gardner et al., 2006; Lipar & Webb, 2015; Murray-Wallace, 1995). This could explain the decrease in aeolian sediment supply to the caves in MIS 5 (Table 4).

High precipitation promotes the growth of denser woody vegetation, which leads to greater connectivity of 'fuel' available for combustion, resulting in increased fire frequency and intensity (Pausas & Paula, 2012). This may explain the peak charcoal deposition in Alexandra Cave between 85 – 72 ka (40 particles/cm<sup>3</sup>). This peak coincides with  $\delta^{13}\text{C}$  depletion, suggesting that plants were becoming increasingly moisture-stressed as a response to increased fire frequency. Similar shifts towards C<sub>4</sub> dominated species following an increase in fire activity have been documented in a global scale study of fire-dependent ecosystems (Bond et al., 2005). Taking into account the low sampling resolution of the  $\delta^{13}\text{C}$  dataset, and that the bulk isotopic value at 325 cm does not lie within the range of individual  $\delta^{13}\text{C}$  values from charcoal pieces (Figure 10), it is likely that more sampling needs to be undertaken in order to fully quantify the palaeoenvironmental conditions derived from Alexandra Cave.

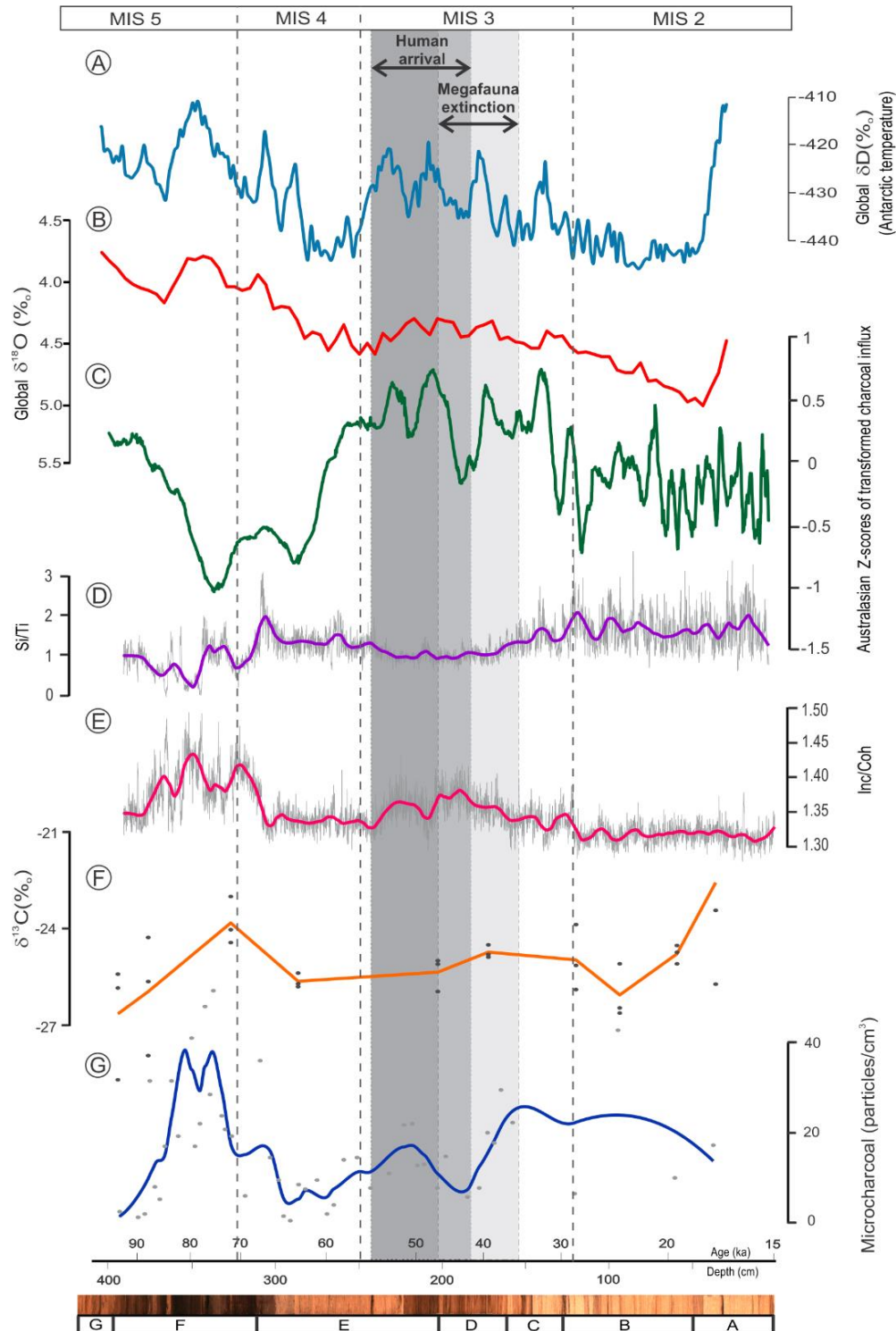


Figure 13. Comparison of Alexandra Cave data with other palaeoclimatic records. Megafauna extinction and human arrival ages derived from Saltré et al. (2016). A. Antarctic temperature ( $\delta D$ ) from EPICA Dome C ice core (EPICA members, 2004) B. Global distributed benthic  $\delta^{18}O$  records from (Lisiecki & Raymo, 2005) C. Australasian charcoal records (z-score of transformed charcoal influx) from Mooney et al. (2011) D. Si/Ti ratio from XRF scanning data at Alexandra Cave sequence. Raw data is represented in grey, and 0.05 LOESS smoothing spline in purple. E. Inc/coh ratio from XRF scanning at Alexandra Cave, used as an indicator of organic matter (pink 0.05 LOESS smoothing spline, raw data in grey) F. Average  $\delta^{13}C$  value of individual charcoal pieces picked from Alexandra Cave G. Micro-charcoal from Alexandra Cave represented as a 0.2 LOESS smoothing spline. Age-depth profile was determined using an age-depth Bayesian model from 'Bacon' package on R v 3.5.0 (Appendix 11). Optical image was produced from the ITRAX<sup>TM</sup> Micro X-ray Fluorescence Core Scanner at ANSTO.



### **Marine Isotope Stage 4 (71 – 57 ka)**

MIS 4 in Alexandra Cave sediments is characterised by low fire frequency. Charcoal and carbon isotope data suggests that it was a period of low biomass burning relative to MIS 5.  $\delta^{13}\text{C}$  enrichment at 65 ka indicates that plants were less moisture-stressed compared to MIS 5 (Figure 13). Sedimentation rate also increased during this time, suggesting increased aeolian input (Table 4). Regional data additionally suggests similar dry conditions. In particular, palaeontological assessments from Cathedral Cave and Grant Hall in NCNP showed a decline in small mammal richness during the MIS 5 - MIS 4 transition, attributed to a response of climatic cooling and drying (Ayliffe et al., 1998). MIS 4 in south-east Australia is characterised by thinning vegetation, low lake levels and dune building (Kershaw et al., 2007; Page et al., 2009; Webb et al., 2014). The increase in inorganic sediment (Si/Ti) and decrease in organic matter (inc/coh) during MIS 4 in Alexandra Cave supports the regional signal of decreased vegetation.

### **Marine Isotope Stage 3 (57 – 29 ka)**

Alexandra Cave sediment showed limited vegetation and geochemical variability during MIS 3, with the exception of a marked increase in biomass burning observed at 42 ka (see discussions below). A decrease in Si input alongside an increase in organic matter suggests a wetter and warmer climate, than MIS 4, although unlikely to be as warm and wet as MIS 5. This interpretation is also supported by the  $\delta^{13}\text{C}$  ratios, which indicates that MIS 3 was more arid than MIS 5 (Figure 13). Low variability in  $\delta^{13}\text{C}$  demonstrate that vegetation did not change markedly, and plants were not particularly moisture-stressed.

In the region, pollen taxa from Blanche Cave documented a high abundance of woody taxa, suggesting wetter conditions. This is concordant with high lake levels in the Willandra Lakes

area of western New South Wales (Bowler et al., 2006). The glacial-interglacial fluctuations observed in the pollen record of Lake Selina and EPICA Dome C ice core (EPICA members., 2004; Petit et al., 1999) during MIS 3 is not observed in the sedimentary deposit of Alexandra Cave, despite a substantial sediment accumulation of 28cm (Figure 4). This could suggest that the sediment accumulation in Alexandra Cave is representative of more localised environmental changes in the region.

### **The Last Glacial Maximum (29 – 17 ka)**

In Alexandra Cave, the Last Glacial Maximum (LGM) is characterised by increased aridity and low biomass burning (Figure 13). The LGM section of Alexandra Cave is visually distinct, with beige coloured sands spanning 1.4 m in height (Figure 4).  $\delta^{13}\text{C}$  values are most enriched during the LGM, and progressively increase over a 15 ka period (-25.2 to -22.4‰), indicating a reduced stomatal conductance, related to drier conditions. The subtle increase in the Si/Ti ratio, and decrease inc/coh ratio, points toward an increase in aeolian input and decrease in organic matter.

During the LGM, Blanche Cave also experienced dry conditions. Darrénougué et al. (2009) reported a decreased sedimentation rate and an increase in herbaceous pollen taxa, with sediment being brought from further inland in a northwest direction. This increase in aridity during the LGM is well documented elsewhere across southern Australia. At Lake Surprise, in south-east Australia, the onset of arid conditions occurred at 28 ka and peaked at 18.5 ka (Falster et al., 2018). A sediment record from Native Companion Lagoon, in south-east Queensland, recorded maximum aeolian sedimentation during the LGM (Petherick et al., 2009). In particular, southern Australia experienced the most arid and coldest conditions during the last glacial cycle, as a result of the northward shift of the polar front, causing in

substantial aeolian accumulation (DeDeckker et al., 2012). This influx in aeolian supply could explain the high sedimentation rate recorded in Alexandra Cave (Table 4).

The absence of Holocene sediment in Alexandra Cave is likely attributed to the chamber reaching full capacity or the cave solution pipe entrance becoming sealed soon after ~15 ka. The latter seems feasible as narrow entrances on the NCNP are prone to blockages by clay soils, rocks and speleothem deposits (Moriarty et al., 2000).

### **Implications for the megafaunal extinction debate**

In Alexandra Cave, the megafaunal extinction window (36.7 – 48.1 ka) (Saltré et al., 2016), is characterised by a change in fire regime (Figure 13). No substantial change was observed in  $\delta^{13}\text{C}$  values and geochemistry, indicating that fairly stable environmental conditions occurred alongside low fire activity between 50 and 43 ka. This period was followed by an increase in regional fire frequency between 43 and 35 ka (Figure 13).

The initial decline in biomass burning (50 – 43 ka) around the time of human arrival (Figure 13) is perplexing, and could potentially reflect climate being a control on the fire regime. A regional compilation of sedimentary charcoal records from Australasia concluded that fire regimes were controlled by climate and climate-induced vegetation changes, and did not correspond with human arrival (Mooney et al., 2011). Taking into account that large continental-scale studies are likely to reflect broad climatic patterns rather than localised impacts by humans, it is unclear if the observed decrease in fire frequency in Alexandra Cave (50 – 43 ka) is a result of human impact or climate.

The subsequent increase in fire during the megafauna extinction window could be interpreted as a contributing factor to their ultimate demise. Systematic burning of landscapes was likely practiced by early human colonisers to clear paths, hunt along fire fronts or promote growth of preferred plants (Miller et al., 2005). This alteration of the landscape, and timing and frequency of biomass burning, could have played a role in the megafauna extinction (Bowman et al., 1998; Prideaux et al., 2010). Alternatively, the increase in fire during the megafauna extinction window could be a response to decreased herbivory pressures, which could have contributed to an increase in fuel stock, and subsequently to increased fire frequency (Prideaux et al., 2010). Lopes dos Santos et al. (2013) demonstrated an increase in biomass burning alongside an increase in C<sub>3</sub> vegetation in southern Australia between 44 – 42 ka, attributing the change in vegetation to decreased herbivory pressure and subsequent increase in fuel for burning. At Lynch's crater, an increase in charcoal is also observed after a decline in *Sporormiella* at 41 ka (Rule et al., 2012). Following the megafauna extinction, this shift in the vegetation regime could have continued, which may have resulted in a sustained higher fire occurrence from 30 to 17 ka in Alexandra Cave (Figure 13).

Importantly, the limited changes in the Alexandra Cave  $\delta^{13}\text{C}$  ratios and geochemical data suggests that local vegetation was not moisture-stressed during the megafauna extinction, despite an increase in fire frequency. A pollen study at Caledonia Fen in the Victorian highlands by Johnson et al., (2016) showed no change in the structure and composition of vegetation during the extinction window. Similarly, Van der Kaars et al. (2017), concluded no temporal association between the extinction and climatically driven environmental changes from a marine core off the south-west shore of Australia. Regionally, Salter et al., (2016) demonstrated that megafauna extinctions were independent of climate aridity and variability over the last 120, 000 years using a combination of proxy and modelling approaches. Limited

evidence for major climatic changes in the region during the extinction window reinforces the complex role fire regimes could have played during the megafauna extinction.

The interpretations presented here are preliminary in nature, and more charcoal data is needed to refine the aforementioned relationships. Nevertheless, initial results suggest a temporal interplay between fire and biodiversity change in the region, either as a cause of or complex response to megafauna demise.

### **Future directions**

This thesis has revealed several new avenues that could be further explored to provide a comprehensive high-resolution environmental record from Alexandra Cave. The ages of ALEX 18-9 and ALEX 18-10 appear to be close to the single-grain OSL dating limits (dose response curve saturation), and it may be more suitable to apply an “extended-range” single-grain dating method such as thermally transferred OSL (TT-OSL) to these samples (Arnold et al., 2015). Additional sampling to include the underlying 1 m of sediment below the current sediment exposure face, would help further refine and potentially extend the chronology of the Alexandra Cave sediment record.

To capture broad changes in MIS 3 – 5, proxy sampling was focused on Units D – F. The next logical step is to further sample Units A – C and G. With the absence of pollen and shells, further study on other environmental proxies such as diatoms and phytoliths might be useful to gain a better understanding of NCNP’s past environmental changes (e.g. Smol et al., 2002). Another useful proxy would be stable carbon isotopes of long-chain n-alkanes from plant leaf waxes, for reconstruction the C<sub>3</sub> - C<sub>4</sub> plant vegetation record and moisture-stress. Measuring levoglucosan, a biomarker produced during burning of vegetation, could

complement the existing charcoal data to reconstruct a biomass burning record in the region (e.g. Lopes dos Santos et al., 2013).

While the XRF data demonstrates changes down the core, it does not provide quantitative values that can aid in pin-pointing sediment sources in the area. Conventional XRF data as spot samples down the core could be used to calibrate qualitative XRF scanner data to quantitative values, from which a more precise provenance of sediment could be derived. Additionally, X-Ray Diffraction (XRD) could provide complementary sediment mineralogy (Arriolabengoa et al., 2015), from which a direct comparison could be made with other caves in NCNP. This type of inter-site geochemical comparison would help shed further light on the sedimentological sources, provenance and post-depositional processes acting between various caves in NCNP.

## CONCLUSION

The detailed sedimentary sequence preserved at Alexandra Cave provides a unique snapshot back in time that offers significant potential for reconstructing the past environment of the region between the Last Glacial Maximum and the last interglacial cycle. From this study, it has been possible to deduce that pollen and *Sporormiella* preservation may be poorly suited to closed caves on NCNP that exhibit small solution pipe openings. In contrast, a range of inorganic and organic proxies that are transported into such caves by surface wash processes rather than airfall offer greater potential for reconstructing palaeoenvironmental histories. Charcoal and carbon isotopes analyses reveal (1) increased aridity during the LGM; (2) absence of major climatic changes during the megafauna extinction window; (3) a potential link between regional fire and megafauna demise; and (4) high fire frequency during MIS 5. The high-resolution XRF scanner provides complementary geochemistry documenting important temporal changes in sediment provenance, cave infill dynamics and organic matter presence.

The palaeoclimate trends observed in this study are in broad agreement with other published climate reconstructions for MIS 5 to 2 in the region, suggesting that the Alexandra Cave sequence primarily reflects external environmental change rather than simply internal cave dynamics. By providing improved reconstructions of past climates and palaeoenvironmental conditions in NCNP using multi-disciplinary approaches, this study has achieved the overarching aim set out in the introduction section (Figure 1), and it has additionally provided new insights into the context and causes of major ecological change occurring in the region during MIS 5 – 2.

To date, only two studies have been conducted on Alexandra Cave sediment: an initial sedimentological study by McCluskey (2012), and the present study on palaeoenvironmental proxies with luminescence dating. Since its discovery, the cave has yielded a number of megafauna bones from disturbed sediment deposits (Reed & Bourne, 2000). The information provided by this study, particularly in elucidating the time range covered by the sequence and the high-resolution nature of the sediment record, demonstrates that a systematic palaeontological excavation of Alexandra Cave is warranted. A detailed palaeontological study on the megafauna fossil deposits, tied together with an in-depth palaeoenvironmental proxy and dating study has the potential to provide much improved reconstructions of fauna-climate interactions occurring in the region between MIS 5 and MIS 2.



## **Acknowledgements**

I would like to thank my supervisors Lee Arnold, Liz Reed and John Tibby for their invaluable feedback and encouragement. A heartfelt thanks goes to Jonathan Tyler and Jenny Reiners, who have supported me over the past few years for this opportunity. Patricia Gadd and ANSTO are thanked for ITRAX scanning. I would also like to thank Mark Rollog and Kristine Nielson for their assistance with carbon isotopes. I am very grateful for the many insightful discussions with Martina Demuro, Haidee Cadd, Richard Lewis, Gilian Ross, Martin Ankor and Christopher Kemp. The Department of Immigration and Border Protection Australia is thanked for the approval of my visa application albeit the 3.5 year wait. Lastly, my parents and partner, James Trezise are thanked for their endless support.

## REFERENCES

- Adetutu, E., Thorpe, K., Shahsavari, E., Bourne, S., Cao, X., Fard, R., . . . Ball, A. (2012). Bacterial community survey of sediments at Naracoorte Caves, Australia. *International Journal of Speleology*, *41*(2), 137-147. doi: 10.5038/1827-806x.41.2.2
- Aitken, M. (1985). *Thermoluminescence dating* (Vol. 359): Academic press London.
- Aitken, M. J. (1998). An Introduction to Optical Dating. *Oxford University Press, Oxford and New York*.
- Arnold, L. J., Demuro, M., Navazo, M., Benito-Calvo, A., & Pérez-González, A. (2013). OSL dating of the Middle Palaeolithic Hotel California site, Sierra de Atapuerca, north-central Spain. *Boreas*, *42*(2), 285-305. doi: doi:10.1111/j.1502-3885.2012.00262.x
- Arnold, L. J., Demuro, M., Parés, J. M., Pérez-González, A., Arsuaga, J. L., Bermúdez de Castro, J. M., & Carbonell, E. (2015). Evaluating the suitability of extended-range luminescence dating techniques over early and Middle Pleistocene timescales: Published datasets and case studies from Atapuerca, Spain. *Quaternary International*, *389*, 167-190. doi: <https://doi.org/10.1016/j.quaint.2014.08.010>
- Arnold, L. J., Demuro, M., & Ruiz, M. N. (2012). Empirical insights into multi-grain averaging effects from 'pseudo' single-grain OSL measurements. *Radiation Measurements*, *47*(9), 652-658. doi: <https://doi.org/10.1016/j.radmeas.2012.02.005>
- Arnold, L. J., Duval, M., Demuro, M., Spooner, N. A., Santonja, M., & Pérez-González, A. (2016). OSL dating of individual quartz 'supergrains' from the Ancient Middle Palaeolithic site of Cuesta de la Bajada, Spain. *Quaternary Geochronology*, *36*, 78-101. doi: <https://doi.org/10.1016/j.quageo.2016.07.003>
- Arnold, L. J., & Roberts, R. G. (2009). Stochastic modelling of multi-grain equivalent dose (De) distributions: Implications for OSL dating of sediment mixtures. *Quaternary Geochronology*, *4*(3), 204-230. doi: <https://doi.org/10.1016/j.quageo.2008.12.001>
- Arnold, L. J., Roberts, R. G., MacPhee, R. D. E., Willerslev, E., Tikhonov, A. N., & Brock, F. (2008). Optical dating of perennially frozen deposits associated with preserved ancient plant and animal DNA in north-central Siberia. *Quaternary Geochronology*, *3*(1), 114-136. doi: <https://doi.org/10.1016/j.quageo.2007.09.002>
- Arriolabengoa, M., Iriarte, E., Aranburu, A., Yusta, I., & Arrizabalaga, A. (2015). Provenance study of endokarst fine sediments through mineralogical and geochemical data (Lezetxiki II cave, northern Iberia). *Quaternary International*, *364*, 231-243. doi: <https://doi.org/10.1016/j.quaint.2014.09.072>
- Aufgebauer, A., Panagiotopoulos, K., Wagner, B., Schaebitz, F., Viehberg, F. A., Vogel, H., . . . Damaschke, M. (2012). Climate and environmental change in the Balkans over the last 17 ka recorded in sediments from Lake Prespa (Albania/F.Y.R. of Macedonia/Greece). *Quaternary International*, *274*, 122-135. doi: <https://doi.org/10.1016/j.quaint.2012.02.015>
- Ayliffe, L. K., Marianelli, P.C., Moriarty, M.C., Wells, R.T., McCulloch, M.T., Mortimer, G.E., Hellstrom, J.C. (1998). 500 ka precipitation record from south-eastern Australia: evidence for interglacial relative aridity. *Geology*, *26*, 147-150.
- Baker, A. G., Bhagwat, S. A., & Willis, K. J. (2013). Do dung fungal spores make a good proxy for past distribution of large herbivores? *Quaternary Science Reviews*, *62*, 21-31. doi: <https://doi.org/10.1016/j.quascirev.2012.11.018>
- Bird, M. I., Turney, C. S. M., Fifield, L. K., Jones, R., Ayliffe, L. K., Palmer, A., . . . Robertson, S. (2002). Radiocarbon analysis of the early archaeological site of Nauwalabila I, Arnhem Land, Australia: implications for sample suitability and stratigraphic integrity. *Quaternary Science Reviews*, *21*(8), 1061-1075. doi: [https://doi.org/10.1016/S0277-3791\(01\)00058-0](https://doi.org/10.1016/S0277-3791(01)00058-0)

- Birks, H. H., & Birks, H. J. B. (2006). Multi-proxy studies in palaeolimnology. *Vegetation History and Archaeobotany*, 15(4), 235-251. doi: 10.1007/s00334-006-0066-6
- Blaauw, M., & Christen, J. A. (2011). Flexible paleoclimate age-depth models using an autoregressive gamma process. *Bayesian Anal.*, 6(3), 457-474. doi: 10.1214/11-BA618
- Blott, S. J., & Pye, K. (2012). Particle size scales and classification of sediment types based on particle size distributions: Review and recommended procedures. *Sedimentology*, 59(7), 2071-2096. doi: 10.1111/j.1365-3091.2012.01335.x
- Bond, W. J., Woodward, F. I., & Midgley, G. F. (2005). The global distribution of ecosystems in a world without fire. *New Phytol*, 165(2), 525-537. doi: 10.1111/j.1469-8137.2004.01252.x
- Bowler, J., Kotsonis, A., & Lawrence, C. R. (2006). *Environmental evolution of the Mallee region, western Murray Basin* (Vol. 118).
- Bowler, J. M., Johnston, H., Olley, J. M., Prescott, J. R., Roberts, R. G., Shawcross, W., & Spooner, N. A. (2003). New ages for human occupation and climatic change at Lake Mungo, Australia. *Nature*, 421(6925), 837.
- Burnett, A. P., Soreghan, M. J., Scholz, C. A., & Brown, E. T. (2011). Tropical East African climate change and its relation to global climate: A record from Lake Tanganyika, Tropical East Africa, over the past 90+kyr. *Palaeogeography, Palaeoclimatology, Palaeoecology*, 303(1), 155-167. doi: https://doi.org/10.1016/j.palaeo.2010.02.011
- Burney, D. A., Robinson, G. S., & Burney, L. P. (2003). Sporormiella and the late Holocene extinctions in Madagascar. *Proceedings of the National Academy of Sciences*, 100(19), 10800-10805. doi: 10.1073/pnas.1534700100
- Carrión, J., Fernández, S., Gonzalez Samperiz, P., Leroy, S. A. G., Bailey, G., López-Sáez, J. A., . . . Dupré, M. (2009). *Quaternary pollen analysis in the Iberian Peninsula: the value of negative results* (Vol. 25).
- Clark, J. S. (1988). Particle Motion and the Theory of Charcoal Analysis: Source Area, Transport, Deposition, and Sampling. *Quaternary Research*, 30(1), 67-80. doi: 10.1016/0033-5894(88)90088-9
- Clark, J. S., & Hussey, T. C. (1996). Estimating the mass flux of charcoal from sedimentary records: effects of particle size, morphology, and orientation. *The Holocene*, 6(2), 129-144. doi: 10.1177/095968369600600201
- Cohen-Ofri, I., Weiner, L., Boaretto, E., Mintz, G., & Weiner, S. (2006). Modern and fossil charcoal: aspects of structure and diagenesis. *Journal of Archaeological Science*, 33(3), 428-439. doi: https://doi.org/10.1016/j.jas.2005.08.008
- Crawford, A. J., & Belcher, C. M. (2014). Charcoal morphometry for paleoecological analysis: The effects of fuel type and transportation on morphological parameters. *Applications in Plant Sciences*, 2(8), apps.1400004. doi: 10.3732/apps.1400004
- Croudace, I. W., & Rothwell, R. G. (2015). Micro-xrf studies of sediment core: Applications of a non-destructive tool for the environmental sciences.
- Czimczik, C. I., Preston, C. M., Schmidt, M. W. I., Werner, R. A., & Schulze, E.-D. (2002). Effects of charring on mass, organic carbon, and stable carbon isotope composition of wood. *Organic Geochemistry*, 33(11), 1207-1223. doi: https://doi.org/10.1016/S0146-6380(02)00137-7
- Darrénougué, N., De Deckker, P., Fitzsimmons, K. E., Norman, M. D., Reed, L., van der Kaars, S., & Fallon, S. (2009). A late Pleistocene record of aeolian sedimentation in Blanche Cave, Naracoorte, South Australia. *Quaternary Science Reviews*, 28(25), 2600-2615. doi: https://doi.org/10.1016/j.quascirev.2009.05.021

- Davis, O. K. (2017). Spores of the Dung Fungus *Sporormiella*: Increased Abundance in Historic Sediments and Before Pleistocene Megafaunal Extinction. *Quaternary Research*, 28(2), 290-294. doi: 10.1016/0033-5894(87)90067-6
- De Deckker, P., Moros, M., Perner, K., & Jansen, E. (2012). Influence of the tropics and southern westerlies on glacial interhemispheric asymmetry. *Nature Geoscience*, 5, 266. doi: 10.1038/ngeo1431
- Diefendorf, A. F., Mueller, K. E., Wing, S. L., Koch, P. L., & Freeman, K. H. (2010). Global patterns in leaf <sup>13</sup>C discrimination and implications for studies of past and future climate. *Proceedings of the National Academy of Sciences*, 107(13), 5738-5743. doi: 10.1073/pnas.0910513107
- Dodson, J. (1975). Vegetation History and Water Fluctuations at Lake Leake, South-Eastern South Australia. II. 50 000 B.P. To 10 000 B.P. *Australian Journal of Botany*, 23(5), 815-831. doi: <https://doi.org/10.1071/BT9750815>
- Dodson, J. (1977). Late Quaternary palaeoecology of Wylie Swamp, southeastern South Australia. *Quaternary Research*, 8(1), 97-114. doi: [https://doi.org/10.1016/0033-5894\(77\)90058-8](https://doi.org/10.1016/0033-5894(77)90058-8)
- Dodson, J., & Field, J. H. (2017). *What does the occurrence of Sporormiella (Preussia) spores mean in Australian fossil sequences?*
- EPICA Members, Augustin, L., Barbante, C., Barnes, P. R. F., Marc Barnola, J., Bigler, M., . . . Zucchelli, M. (2004). Eight glacial cycles from an Antarctic ice core. *Nature*, 429, 623. doi: 10.1038/nature02599
- Falster, G., Tyler, J., Grant, K., Tibby, J., Turney, C., Löhr, S., . . . Kershaw, A. P. (2018). Millennial-scale variability in south-east Australian hydroclimate between 30,000 and 10,000 years ago. *Quaternary Science Reviews*, 192, 106-122. doi: <https://doi.org/10.1016/j.quascirev.2018.05.031>
- Forbes, & Bestland, E. A. (2007). Origin of the sedimentary deposits of the Naracoorte Caves, South Australia. *Geomorphology*, 86(3), 369-392. doi: <https://doi.org/10.1016/j.geomorph.2006.09.009>
- Forbes, M. S., Bestland, E. A., Wells, R. T., & Krull, E. S. (2007). Palaeoenvironmental reconstruction of the Late Pleistocene to Early Holocene Robertson Cave sedimentary deposit, Naracoorte, South Australia. *Australian Journal of Earth Sciences*, 54(4), 541-559. doi: 10.1080/08120090601078388
- Galbraith, R. F., & Roberts, R. G. (2012). Statistical aspects of equivalent dose and error calculation and display in OSL dating: An overview and some recommendations. *Quaternary Geochronology*, 11, 1-27. doi: <https://doi.org/10.1016/j.quageo.2012.04.020>
- Galbraith, R. F., Roberts, R. G., Laslett, G. M., Yoshida, H., & Olley, J. M. (1991). Optical dating of single and multiple grains of quartz from jinnium rock shelter, northern australia: part i, experimental design and statistical models\*. *Archaeometry*, 41(2), 339-364. doi: 10.1111/j.1475-4754.1999.tb00987.x
- Gardner, T. W., Webb, J., Davis, A. G., Cassel, E. J., Pezzia, C., Merritts, D. J., & Smith, B. (2006). Late Pleistocene landscape response to climate change: aeolian and alluvial fan deposition, Cape Liptrap, southeastern Australia. *Quaternary Science Reviews*, 25(13), 1552-1569. doi: <https://doi.org/10.1016/j.quascirev.2005.12.003>
- Grant, K. M., Rohling, E. J., Westerhold, T., Zabel, M., Heslop, D., Konijnendijk, T., & Lourens, L. (2017). A 3 million year index for North African humidity/aridity and the implication of potential pan-African Humid periods. *Quaternary Science Reviews*, 171, 100-118. doi: <https://doi.org/10.1016/j.quascirev.2017.07.005>

- Grün, R., Moriarty, K., & Wells, R. (2001). Electron spin resonance dating of the fossil deposits in the Naracoorte Caves, South Australia. *Journal of Quaternary Science*, 16(1), 49-59.
- Guérin, G., Mercier, N., & Adamiec, G. (2011). Dose-rate conversion factors: update. *Ancient tL*, 29(1), 5-8.
- Guyard, H., Chapron, E., St-Onge, G., Anselmetti, F. S., Arnaud, F., Magand, O., . . . Mélières, M.-A. (2007). High-altitude varve records of abrupt environmental changes and mining activity over the last 4000 years in the Western French Alps (Lake Bramant, Grandes Rousses Massif). *Quaternary Science Reviews*, 26(19), 2644-2660. doi: <https://doi.org/10.1016/j.quascirev.2007.07.007>
- Hamm, G., Mitchell, P., Arnold, L. J., Prideaux, G. J., Questiaux, D., Spooner, N. A., . . . Johnston, D. (2016). Cultural innovation and megafauna interaction in the early settlement of arid Australia. *Nature*, 539, 280. doi: 10.1038/nature20125
- Department for Environment and Heritage. (2001). *Naracoorte Caves National Park management plan, South East, South Australia*. [Adelaide]: Dept. for Environment and Heritage.
- Hogg, A. G., Hua, Q., Blackwell, P. G., Niu, M., Buck, C. E., Guilderson, T. P., . . . Zimmerman, S. R. H. (2013). SHCal13 Southern Hemisphere Calibration, 0–50,000 Years cal BP. *Radiocarbon*, 55(4), 1889-1903. doi: 10.2458/azu\_js\_rc.55.16783
- Hunt, C. O., & Fiacconi, M. (2018). Pollen taphonomy of cave sediments: What does the pollen record in caves tell us about external environments and how do we assess its reliability? *Quaternary International*, 485, 68-75. doi: <https://doi.org/10.1016/j.quaint.2017.05.016>
- Huntley, D. J., Godfrey-Smith, D. I., & Thewalt, M. L. W. (1985). Optical dating of sediments. *Nature*, 313, 105. doi: 10.1038/313105a0
- Huntley, D. J., & Lamothe, M. (2001). Ubiquity of anomalous fading in K-feldspars and the measurement and correction for it in optical dating. *Canadian Journal of Earth Sciences*, 38(7), 1093-1106. doi: 10.1139/e01-013
- Jacobs, Z., & Roberts, R. G. (2008). Advances in optically stimulated luminescence dating of individual grains of quartz from archeological deposits. *Evolutionary Anthropology: Issues, News, and Reviews*, 16(6), 210-223. doi: 10.1002/evan.20150
- Johnson, C. N., Rule, S., Haberle, S. G., Kershaw, A. P., McKenzie, G. M., & Brook, B. W. (2015). Geographic variation in the ecological effects of extinction of Australia's Pleistocene megafauna. *Ecography*, 39(2), 109-116. doi: 10.1111/ecog.01612
- Jouve, G., Francus, P., Lamoureux, S., Provencher-Nolet, L., Hahn, A., Haberzettl, T., . . . Nuttin, L. (2013). Microsedimentological characterization using image analysis and  $\mu$ -XRF as indicators of sedimentary processes and climate changes during Lateglacial at Laguna Potrok Aike, Santa Cruz, Argentina. *Quaternary Science Reviews*, 71, 191-204. doi: <https://doi.org/10.1016/j.quascirev.2012.06.003>
- Kershaw, A. P., McKenzie, G. M., Porch, N., Roberts, R. G., Brown, J., Heijnis, H., . . . Newall, P. R. (2007). A high-resolution record of vegetation and climate through the last glacial cycle from Caledonia Fen, southeastern highlands of Australia. *Journal of Quaternary Science*, 22(5), 481-500. doi: 10.1002/jqs.1127
- Lipar, M., & Webb, J. (2015). The Middle & Late Pleistocene Bridgewater Formation on Cape Bridgewater, south-western Victoria: chronostratigraphy and palaeoclimatic significance. *Proceedings of the Royal Society of Victoria*, 127(2), 81-91. doi: <https://doi.org/10.1071/RS15020>
- Lisiecki, L. E., & Raymo, M. E. (2005). *Pliocene-Pleistocene stack of globally distributed benthic stable oxygen isotope records*. Retrieved from: <https://doi.org/10.1594/PANGAEA.704257>

- Lopes dos Santos, R. A., De Deckker, P., Hopmans, E. C., Magee, J. W., Mets, A., Sinninghe Damsté, J. S., & Schouten, S. (2013). Abrupt vegetation change after the Late Quaternary megafaunal extinction in southeastern Australia. *Nature Geoscience*, *6*, 627. doi: 10.1038/ngeo1856
- Lynch, J. A., Clark, J. S., & Stocks, B. J. (2004). Charcoal production, dispersal, and deposition from the Fort Providence experimental fire: interpreting fire regimes from charcoal records in boreal forests. *Canadian Journal of Forest Research*, *34*(8), 1642-1656. doi: 10.1139/x04-071
- Macken, A. C., Jankowski, N. R., Price, G. J., Bestland, E. A., Reed, E. H., Prideaux, G. J., & Roberts, R. G. (2011). Application of sedimentary and chronological analyses to refine the depositional context of a Late Pleistocene vertebrate deposit, Naracoorte, South Australia. *Quaternary Science Reviews*, *30*(19), 2690-2702. doi: <https://doi.org/10.1016/j.quascirev.2011.05.023>
- Macken, A. C., Prideaux, G. J., & Reed, E. H. (2012). Variation and pattern in the responses of mammal faunas to Late Pleistocene climatic change in southeastern South Australia. *Journal of Quaternary Science*, *27*(4), 415-424. doi: 10.1002/jqs.1563
- Macken, A. C., Staff, R. A., & Reed, E. H. (2013). Bayesian age-depth modelling of Late Quaternary deposits from Wet and Blanche Caves, Naracoorte, South Australia: A framework for comparative faunal analyses. *Quaternary Geochronology*, *17*, 26-43. doi: <https://doi.org/10.1016/j.quageo.2013.03.001>
- McCluskey, C. (2012). Cave sediments as Palaeoenvironmental Indicators: Alexandra Cave, Naracoorte, South Australia. *Honours Thesis, Australian National University*.
- Miller, G. H., Fogel, M. L., Magee, J. W., Gagan, M. K., Clarke, S. J., & Johnson, B. J. (2005). Ecosystem Collapse in Pleistocene Australia and a Human Role in Megafaunal Extinction. *Science*, *309*(5732), 287-290.
- Mooney, S. D., Harrison, S. P., Bartlein, P. J., Daniau, A. L., Stevenson, J., Brownlie, K. C., . . . Williams, N. (2011). Late Quaternary fire regimes of Australasia. *Quaternary Science Reviews*, *30*(1), 28-46. doi: <https://doi.org/10.1016/j.quascirev.2010.10.010>
- Moore, P. D., Webb, J.A. . (1978). An illustrated Guide to pollen analysis. *Hodder and Stoughton*. doi: [https://doi.org/10.1016/0034-6667\(81\)90025-7](https://doi.org/10.1016/0034-6667(81)90025-7)
- Moriarty, K. C., McCulloch, M. T., Wells, R. T., & McDowell, M. C. (2000). Mid-Pleistocene cave fills, megafaunal remains and climate change at Naracoorte, South Australia: towards a predictive model using U-Th dating of speleothems. *Palaeogeography, Palaeoclimatology, Palaeoecology*, *159*(1), 113-143. doi: [https://doi.org/10.1016/S0031-0182\(00\)00036-5](https://doi.org/10.1016/S0031-0182(00)00036-5)
- Munsell. (2010). *Munsell soil color charts : with genuine Munsell color chips: 2009 year revised*. Grand Rapids, MI : Munsell Color, 2010.
- Murray-Wallace, C. V. (1995). Aminostratigraphy of Quaternary coastal sequences in southern Australia — An overview. *Quaternary International*, *26*, 69-86. doi: [https://doi.org/10.1016/1040-6182\(94\)00048-A](https://doi.org/10.1016/1040-6182(94)00048-A)
- Murray, A. S., & Wintle, A. G. (2000). Luminescence dating of quartz using an improved single-aliquot regenerative-dose protocol. *Radiation Measurements*, *32*(1), 57-73. doi: [https://doi.org/10.1016/S1350-4487\(99\)00253-X](https://doi.org/10.1016/S1350-4487(99)00253-X)
- Nelson, M. S., Gray, H. J., Johnson, J. A., Rittenour, T. M., Feathers, J. K., & Mahan, S. A. (2017). User Guide for Luminescence Sampling in Archaeological and Geological Contexts. *Advances in Archaeological Practice*, *3*(2), 166-177. doi: 10.7183/2326-3768.3.2.166
- Page, K. J., Kemp, J., & Nanson, G. C. (2009). Late Quaternary evolution of Riverine Plain paleochannels, southeastern Australia. *Australian Journal of Earth Sciences*, *56*(sup1), S19-S33. doi: 10.1080/08120090902870772

- Pausas, J. G., & Paula, S. (2012). Fuel shapes the fire–climate relationship: evidence from Mediterranean ecosystems. *Global Ecology and Biogeography*, *21*(11), 1074-1082. doi: 10.1111/j.1466-8238.2012.00769.x
- Petherick, L. M., McGowan, H. A., & Kamber, B. S. (2009). Reconstructing transport pathways for late Quaternary dust from eastern Australia using the composition of trace elements of long traveled dusts. *Geomorphology*, *105*(1), 67-79. doi: <https://doi.org/10.1016/j.geomorph.2007.12.015>
- Petit, J. R., Jouzel, J., Raynaud, D., Barkov, N. I., Barnola, J. M., Basile, I., . . . Stievenard, M. (1999). Climate and atmospheric history of the past 420,000 years from the Vostok ice core, Antarctica. *Nature*, *399*, 429. doi: 10.1038/20859
- Prescott, J. R., & Hutton, J. T. (1994). Cosmic ray contributions to dose rates for luminescence and ESR dating: Large depths and long-term time variations. *Radiation Measurements*, *23*(2), 497-500. doi: [https://doi.org/10.1016/1350-4487\(94\)90086-8](https://doi.org/10.1016/1350-4487(94)90086-8)
- Prescott, J. R., & Hutton, J. T. (1995). Environmental dose rates and radioactive disequilibrium from some Australian luminescence dating sites. *Quaternary Science Reviews*, *14*(4), 439-448. doi: [https://doi.org/10.1016/0277-3791\(95\)00037-2](https://doi.org/10.1016/0277-3791(95)00037-2)
- Price, G. J., Ferguson, K. J., Webb, G. E., Feng, Y.-x., Higgins, P., Nguyen, A. D., . . . Louys, J. (2017). Seasonal migration of marsupial megafauna in Pleistocene Sahul (Australia–New Guinea). *Proceedings of the Royal Society B: Biological Sciences*, *284*(1863). doi: 10.1098/rspb.2017.0785
- Prideaux, G. J., Gully, G. A., Couzens, A. M. C., Ayliffe, L. K., Jankowski, N. R., Jacobs, Z., . . . Hatcher, L. M. (2010). Timing and dynamics of Late Pleistocene mammal extinctions in southwestern Australia. *Proceedings of the National Academy of Sciences*, *107*(51), 22157-22162. doi: 10.1073/pnas.1011073107
- Prideaux, G. J., Roberts, R. G., Megirian, D., Westaway, K. E., Hellstrom, J. C., & Olley, J. M. (2007). Mammalian responses to Pleistocene climate change in southeastern Australia. *Geology*, *35*(1), 33-36. doi: 10.1130/G23070A.1
- Reed, E., & Bourne, S. (2000). *Pleistocene fossil vertebrate sites of the South-East region of South Australia* (Vol. 124).
- Roberts, R. G., Flannery, T. F., Ayliffe, L. K., Yoshida, H., Olley, J. M., Prideaux, G. J., . . . Smith, B. L. (2001). New Ages for the Last Australian Megafauna: Continent-Wide Extinction About 46,000 Years Ago. *Science*, *292*(5523), 1888-1892. doi: 10.1126/science.1060264
- Roberts, R. G., Jacobs, Z., Li, B., Jankowski, N. R., Cunningham, A. C., & Rosenfeld, A. B. (2015). Optical dating in archaeology: thirty years in retrospect and grand challenges for the future. *Journal of Archaeological Science*, *56*, 41-60. doi: <https://doi.org/10.1016/j.jas.2015.02.028>
- Rule, S., Brook, B. W., Haberle, S. G., Turney, C. S. M., Kershaw, A. P., & Johnson, C. N. (2012). The Aftermath of Megafaunal Extinction: Ecosystem Transformation in Pleistocene Australia. *Science*, *335*(6075), 1483-1486.
- Saltré, F., Rodríguez-Rey, M., Brook, B. W., Johnson, C. N., Turney, C. S. M., Alroy, J., . . . Bradshaw, C. J. A. (2016). Climate change not to blame for late Quaternary megafauna extinctions in Australia. *Nature Communications*, *7*, 10511. doi: 10.1038/ncomms10511
- Schleser, G. H., Frielingsdorf, J., & Blair, A. (1999). Carbon isotope behaviour in wood and cellulose during artificial aging. *Chemical Geology*, *158*(1), 121-130. doi: [https://doi.org/10.1016/S0009-2541\(99\)00024-8](https://doi.org/10.1016/S0009-2541(99)00024-8)
- Schneider, C. A., Rasband, W. S., & Eliceiri, K. W. (2012). NIH Image to ImageJ: 25 years of image analysis. *Nature Methods*, *9*, 671. doi: 10.1038/nmeth.2089

- Service, S. A. N. P. a. W. (1986). Draft Management Plan: Naracoorte Caves Conservation Park.
- Shala, S., Helmens, K. F., Jansson, K. N., Kylander, M. E., Risberg, J., & Löwemark, L. (2013). Palaeoenvironmental record of glacial lake evolution during the early Holocene at Sokli, NE Finland. *Boreas*, 43(2), 362-376. doi: 10.1111/bor.12043
- Smol, J. P., Birks, H. J. B., & Last, W. M. (2002). *Tracking Environmental Change Using Lake Sediments, Volume 3 : Terrestrial, Algal, and Siliceous Indicators*. Dordrecht, NETHERLANDS: Kluwer Academic Publishers.
- St Pierre, E., Zhao, J., Feng, Y., & Reed, E. (2012). U-series dating of soda straw stalactites from excavated deposits: method development and application to Blanche Cave, Naracoorte, South Australia. *Journal of Archaeological Science*, 39(4), 922-930. doi: <https://doi.org/10.1016/j.jas.2011.10.027>
- Turekian, V. C., Macko, S., Ballentine, D., Swap, R. J., & Garstang, M. (1998). Causes of bulk carbon and nitrogen isotopic fractionations in the products of vegetation burns: laboratory studies. *Chemical Geology*, 152(1), 181-192. doi: [https://doi.org/10.1016/S0009-2541\(98\)00105-3](https://doi.org/10.1016/S0009-2541(98)00105-3)
- Turney, C. (2012). Surface  $\delta^{13}\text{C}$  in Australia: A quantified measure of annual precipitation? *Peopled Landscapes* (Vol. 34, pp. 435-444): ANU Press.
- Turney, C., Wheeler, D., & Chivas, A. R. (2006). Carbon isotope fractionation in wood during carbonization. *Geochimica et Cosmochimica Acta*, 70(4), 960-964. doi: <https://doi.org/10.1016/j.gca.2005.10.031>
- Van der Kaars, S., Miller, G., Turney, C. M., Cook, E., Nürnberg, D. J., Kershaw, P., Lehman, S. (2017). Humans rather than climate the primary cause of Pleistocene megafaunal extinction in Australia. *Nature Communications*, 8, 14142. doi: 10.1038/ncomms14142
- Van der Kaars, W. A. (1991). Palynology of eastern Indonesian marine piston-cores: a Late Quaternary vegetational and climatic record for Australasia. *Palaeogeography, Palaeoclimatology, Palaeoecology*, 85(3), 239-302. doi: [https://doi.org/10.1016/0031-0182\(91\)90163-L](https://doi.org/10.1016/0031-0182(91)90163-L)
- Webb, M., Dredge, J., Barker, P. A., MÜLLer, W., Jex, C., Desmarchelier, J., . . . Wynn, P. M. (2014). Quaternary climatic instability in south-east Australia from a multi-proxy speleothem record. *Journal of Quaternary Science*, 29(6), 589-596. doi: 10.1002/jqs.2734
- Weltje, G. J., & Tjallingii, R. (2008). Calibration of XRF core scanners for quantitative geochemical logging of sediment cores: Theory and application. *Earth and Planetary Science Letters*, 274(3-4), 423-438. doi: 10.1016/j.epsl.2008.07.054
- White, S., & Webb, J. A. (2015). The influence of tectonics on flank margin cave formation on a passive continental margin: Naracoorte, Southeastern Australia. *Geomorphology*, 229, 58-72. doi: <https://doi.org/10.1016/j.geomorph.2014.09.003>
- Wood, J. R., Wilmshurst, J. M., Worthy, T. H., & Cooper, A. (2011). *Sporormiella* as a proxy for non-mammalian herbivores in island ecosystems. *Quaternary Science Reviews*, 30(7), 915-920. doi: <https://doi.org/10.1016/j.quascirev.2011.01.007>
- Wroe, S., Field, J. H., Archer, M., Grayson, D. K., Price, G. J., Louys, J., . . . Mooney, S. D. (2013). Climate change frames debate over the extinction of megafauna in Sahul (Pleistocene Australia-New Guinea). *Proceedings of the National Academy of Sciences*, 110(22), 8777.



## APPENDIX

### Appendix 1: Radiocarbon ages from Alexandra Cave

Radiocarbon ( $^{14}\text{C}$ ) ages have previously been obtained for the uppermost part of the Alexandra Cave sediment sequence by McCluskey (2012) and Reed (Personal communication, 2018). The charcoal fragments were pre-treated using the acid-base-acid method and converted to graphite following Australian National University (ANU) Research School of Earth Sciences' protocol. Samples were packed into pellets and measured on the ANU Single Stage Accelerator Mass Spectrometer.  $^{14}\text{C}$  ages were initially calibrated to calendar ages using OxCal 4.1 online and the Int Cal 09 calibration curve in the original study of McCluskey (2012). However, the calendar ages presented here have been recalibrated using the SHCal 13 curve in OxCal 4.3, which is a more appropriate calibration curve for samples originated from the Southern Hemisphere (Hogg et al., 2013).

| Sample Name | SANU sample # | Location depth (cm) | $^{14}\text{C}$ Conventional age $\pm 1\sigma$ error ( $^{14}\text{C}$ yr BP) | Calendar Age (Cal. Yr BP 95.4 % confidence interval) | Sample weight (mg) | % carbon | Age acquired by |
|-------------|---------------|---------------------|---|--|--------------------|----------|-----------------|
| B8          | 27706         | 185                 | 26150 $\pm$ 175   | 29830 to 30826                                       | 6.03               | 16       | McCluskey       |
| A4          | 27707         | 180                 | 23260 $\pm$ 100   | 27286 to 27690                                       | 11.7               | 17       | McCluskey       |
| A7          | 27709         | 130                 | 17600 $\pm$ 70  | 20945 to 21489                                       | 56.8               | 34       | McCluskey       |
| A13         | 26627         | 70                  | 14588 $\pm$ 53  | 17539 to 17925                                       | 7.3                | 46       | McCluskey       |

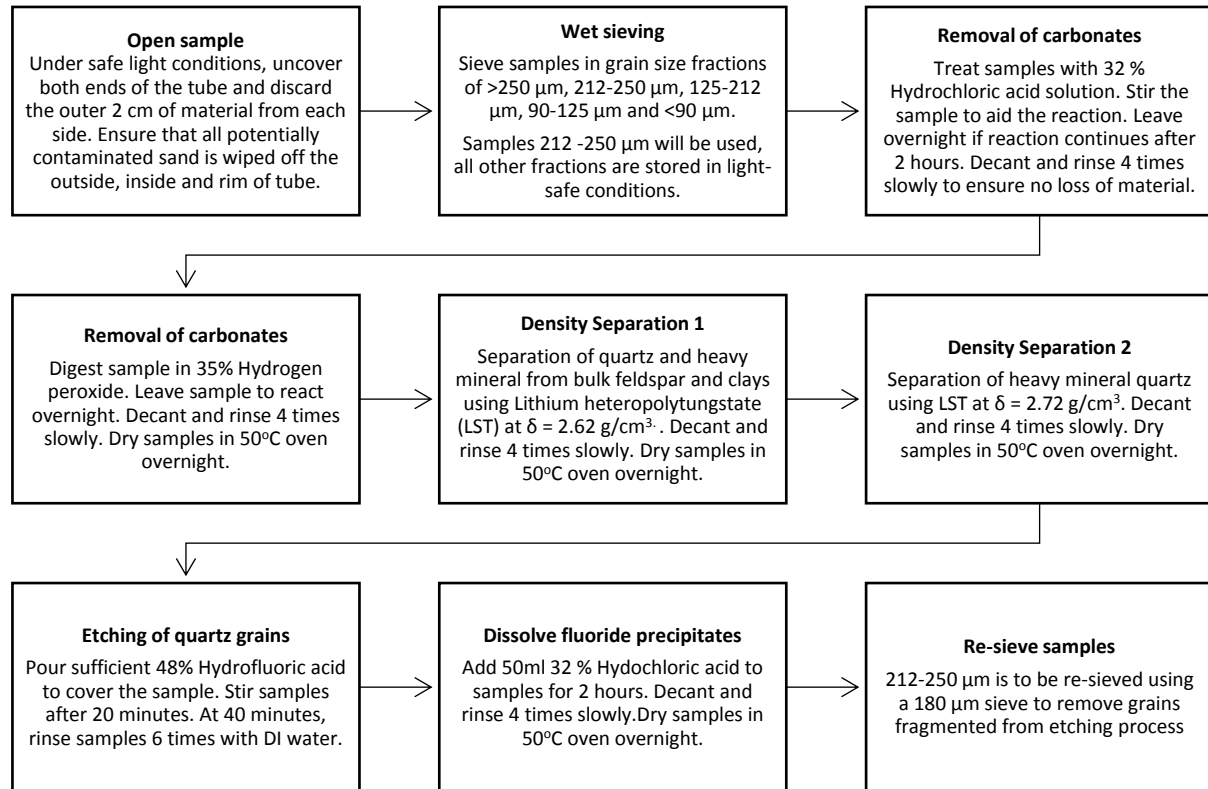
## Appendix 2: OSL sampling in field

Field photo of ALEX 18-4, ALEX 18-5 and ALEX 18-6 OSL samples. An opaque metal cylinder is shown hammered into the sample position of ALEX 18-4. ALEX 18-5 and ALEX 18-6 have already been sampled and are covered with plastic bags to ensure no loss in moisture while awaiting measurement by field gamma spectrometer. Field gamma irradiation measurements were made using a portable gamma spectrometer NaI:Tl detector connected to InInspector 1000 digital handheld multichannel analyser.



### Appendix 3: OSL sample procedure

OSL sample preparation procedure in Prescott Environmental Luminescence Laboratory at the University of Adelaide. OSL lab sampling procedure chart. Each sample was processed under safe light (605 nm,  $<0.15 \mu\text{W}/\text{cm}^2$ ) conditions, using standard laboratory procedures outlined (Aitken, 1985) .



#### **Appendix 4: OSL equipment setting**

Measurements were made using a Risø TL-DA-20 reader equipped with a  $^{90}\text{Sr}/^{90}\text{Y}$  beta source that had been calibrated to administer known doses to multi-grain aliquots and single-grain discs (average single-grain dose rate at the time of measurement = 0.1 Gy/s). OSL signals were each detected using an EMI 9235QA photomultiplier tube, fitted with a 7.5 mm-thick Hoya U-340 filters. Spatial variations in the beta dose rate across the disc plane were taken into account by undertaking hole-specific calibrations using gamma-irradiated quartz (Arnold et al., 2012). An initial dose-response test was conducted on multi-grain disks at 3mm masks to determine appropriate test dose pre-heat temperatures of 220°C. Using the Single-Aliquot Regenerative-dose (SAR) procedure, 500 individual grains of each sample were measured in aluminium discs for  $D_e$  determination.

The environmental dose rate is derived from the external gamma, beta and cosmic dose rates in the surrounding environment. Field gamma irradiation measurements were made using a portable gamma spectrometer NaI:Tl detector connected to InSpector 1000 digital handheld multichannel analyser. The gamma detector is fitted into holes made for OSL sample collection for 45 minutes each, with the exception of ALEX 18-6, which was measured for 60 minutes.

External beta dose rates were calculated from measurements made on a Risø GM-25-5 beta counter, using homogenised sediment sub-samples collected from the main luminescence dating sample positions. Standards of known beta dose rates (MgO and Nussi) were used to convert beta count rates into beta dose rates using the conversion factors of Guerin et al. (2011).

Cosmic-ray dose rates were calculated using the approach described in Prescott and Hutton (1994), taking into consideration the site altitude, geomagnetic latitude as well as the density, thickness and geometry of sediment and bedrock above the sample. The gamma, beta and cosmic-ray dose rates are corrected for long-term sediment water content (Aitken, 1985).

## Appendix 5: Single-Aliquot Regenerative (SAR) Protocol

Following Arnold et al. (2013, 2016), single-grain  $D_e$  estimates were rejected if they exhibited one or more of the following properties:

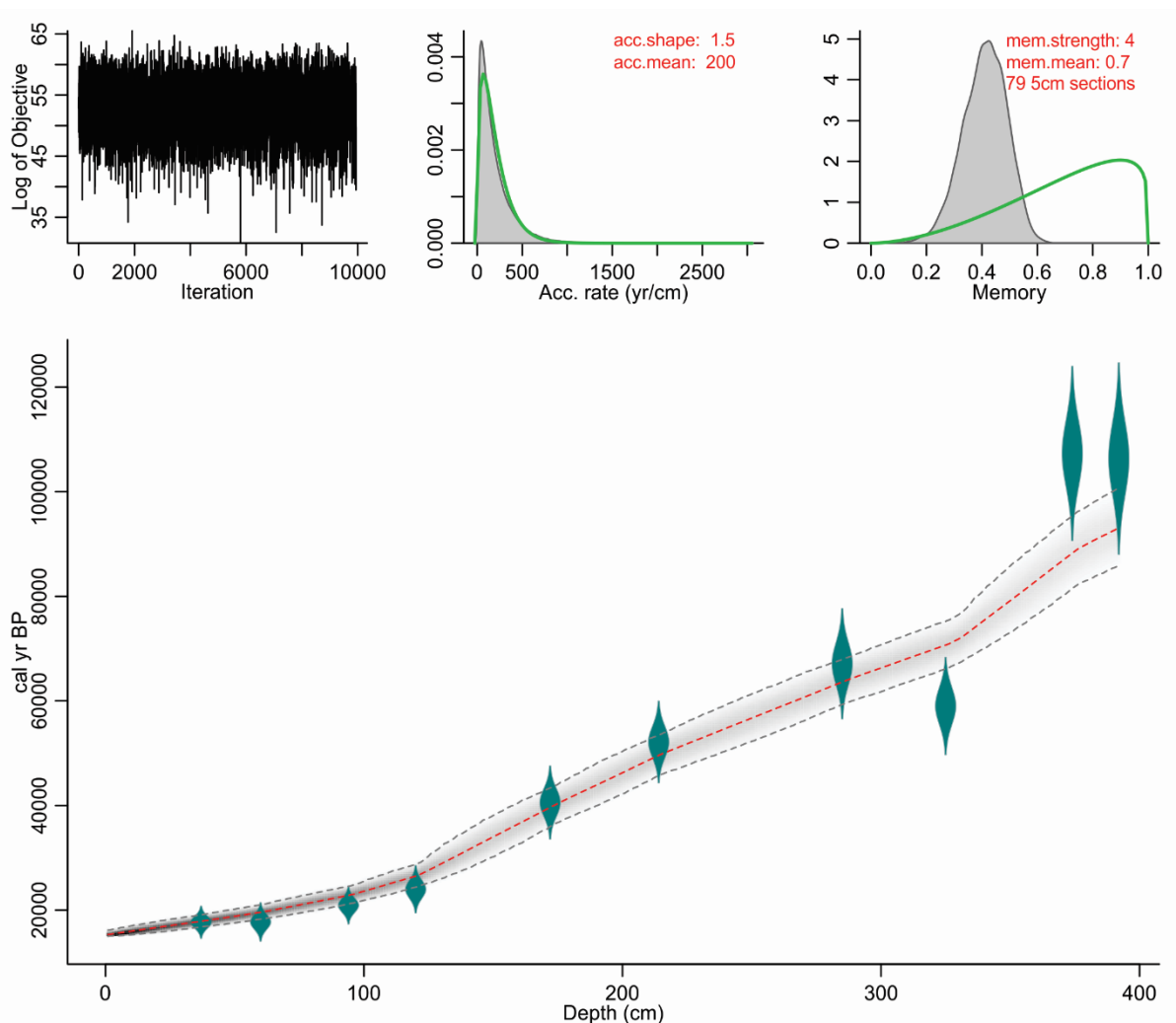
- (1) weak OSL signal (intensity of the natural test-dose signal ( $T_n$ ) is less than three times the standard deviation of the late-light background signal);
- (2) poor recycling ratios (ratios of sensitivity-corrected luminescence responses ( $L_x/T_x$ ) for two identical regenerative doses  $\neq 1 \pm 2\sigma$ )
- (3) high levels of signal recuperation (sensitivity-corrected luminescence response of the 0 Gy regenerative dose point amounted to  $>5\%$  of the sensitivity-corrected natural signal response ( $L_n/T_n$ ))
- (4) saturated or non-intersecting natural OSL signals ( $L_n/T_n$  values equal to, or greater than, the saturation limit of the dose-response curve)
- (5) Max test dose error  $>30\%$
- (6) Contamination by feldspars (ratio of the  $L_x/T_x$  values for two identical regenerative doses measured before and after IR stimulation  $\neq 1 \pm 2\sigma$ ).
- (7) Anomalous dose-response curves (Curves displaying negative response or scattered  $L_x/T_x$  values that could not be successfully fitted with the Monte Carlo procedure)

Table below represents number of rejected grains that fail the abovementioned SAR criteria, total number of grains rejected, and number of grains accepted for each sample.

| SAR criteria | ALEX 18-1 | ALEX 18-2 | ALEX 18-3 | ALEX 18-4 | ALEX 18-5 | ALEX 18-6 | ALEX 18-7 | ALEX 18-8 | ALEX 18-9 | ALEX 18-10 |
|--------------|-----------|-----------|-----------|-----------|-----------|-----------|-----------|-----------|-----------|------------|
| (1)          | 138       | 166       | 117       | 139       | 112       | 90        | 106       | 123       | 98        | 113        |
| (2)          | 61        | 61        | 74        | 73        | 96        | 91        | 67        | 78        | 72        | 69         |
| (3)          | 4         | 2         | 4         | 4         | 4         | 5         | 6         | 8         | 4         | 1          |
| (4)          | 7         | 0         | 0         | 0         | 9         | 9         | 8         | 15        | 93        | 28         |
| (5)          | 2         | 46        | 57        | 40        | 33        | 44        | 48        | 41        | 23        | 46         |
| (6)          | 18        | 21        | 12        | 22        | 13        | 16        | 14        | 15        | 15        | 13         |
| (7)          | 96        | 83        | 123       | 115       | 118       | 139       | 120       | 101       | 98        | 153        |
| Rejected     | 326       | 379       | 387       | 393       | 385       | 394       | 369       | 381       | 403       | 423        |
| Accepted     | 174       | 121       | 113       | 107       | 115       | 106       | 131       | 119       | 97        | 77         |

## Appendix 6: Bayesian age-depth model

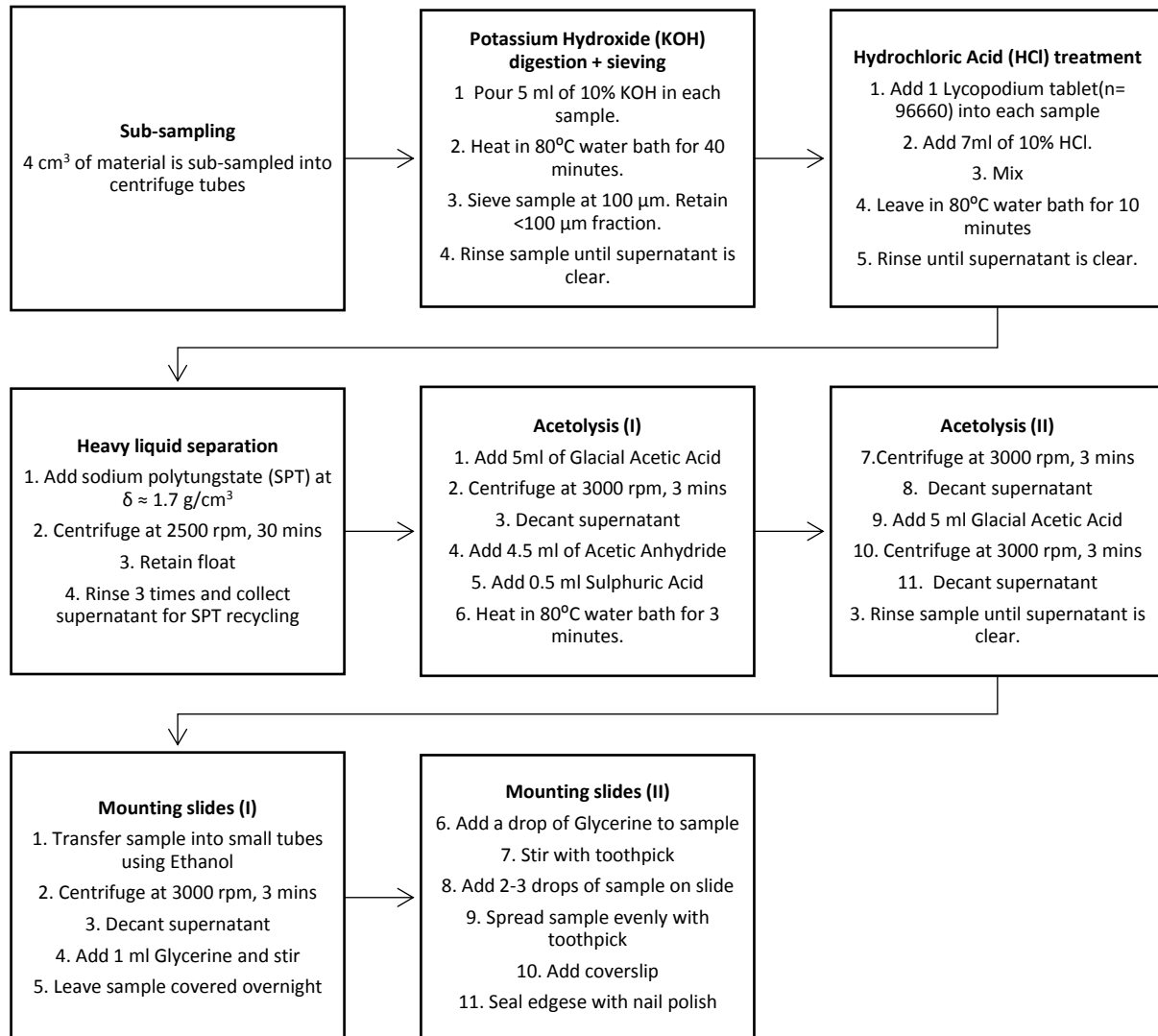
Age-depth modelling using Bayesian statistics to reconstruct accumulation histories for deposits using OSL ages and depth information in ‘Bacon’ program on R v 3.5.1. The model ran 17,820,000 Markov Chain Monte Carlo (MCMC) iterations to estimate mean ages down the sequence. Estimates starting date of accumulation is set at 15 ka, the minimum age of the first OSL sample, ALEX 18-1. 90% of the ages lie within the age-depth model’s 95% CI range. This model is not presented in the main body of thesis. The underlying assumption of this model is that sedimentation rate is continuous, which may not necessarily be the case for all cave sediment infill sequences.



Bacon output graph. Upper left panel depicts the MCMC iterations, the middle panel shows distributions for accumulation rate (prior: green curve, posterior: grey histogram) and memory (right panel). Bottom panel shows calibrated OSL ages (green at  $\pm 2$  sigma uncertainty range), and the age-depth model (grey dotted line shows 95% confidence intervals; red line shows ‘best’ model based on weighted mean age for each depth).

## Appendix 7: Pollen sample procedure

4cm<sup>3</sup> of each sample was sieved at 250µm. The >250 µm samples were bleached in 10% H<sub>2</sub>O<sub>2</sub> for 24 hours and photographed to identify macrocharcoal particles (Appendix 3). The <250 µm pollen, charcoal and *Sporormiella* sample processing procedure is outlined below. This procedure is adapted from a modified protocol from Moore & Webb 1978.



## Appendix 8: Macro-charcoal set-up

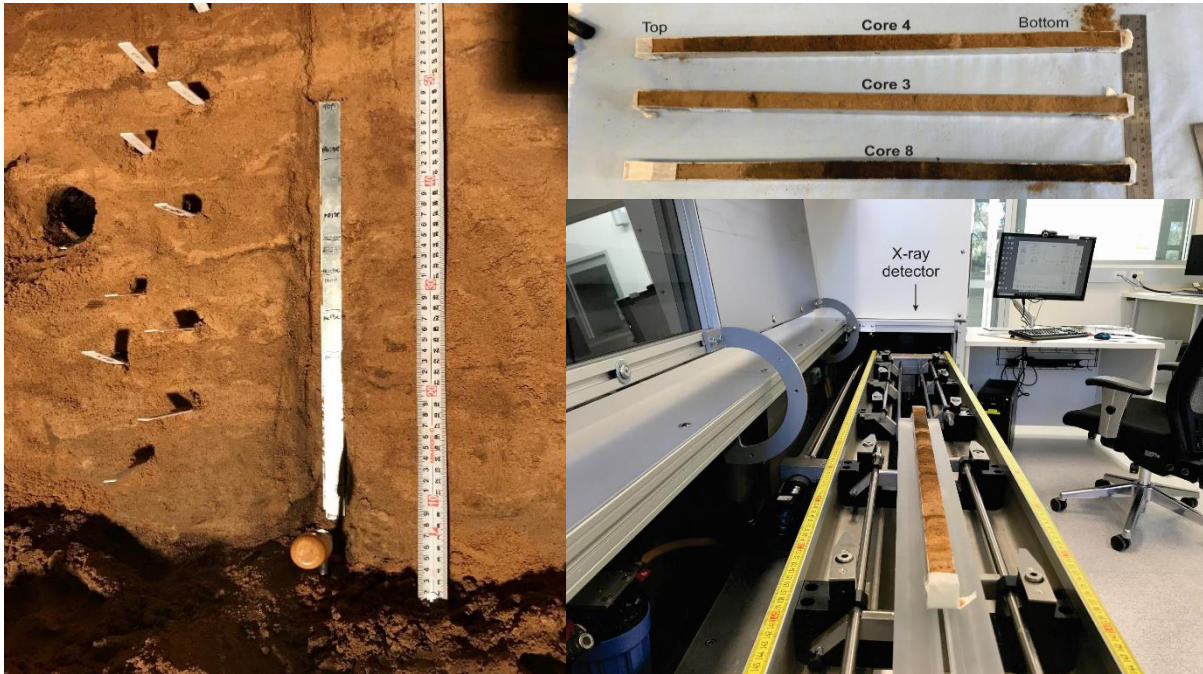
>250  $\mu\text{m}$  samples were bleached in 10% hydrogen peroxide for 24 hours, placed in a petri dish and imaged under a light box. Each image is taken with sample name and a black ruler for scale. Images are transferred to a photo imaging software, ImageJ. Area of black charcoal particles are measured by adjusting the threshold colours. Photography set up and sample photo below.








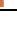










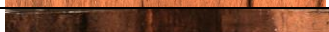



## Appendix 9: ITRAX™ XRF core scanning

Field photos of sediment core acquisition and in-lab measurement set up of ITRAX™ Micro X-ray Fluorescence Core Scanner at the Australian Nuclear Science and Technology Organisation (ANSTO) facility. Measurements were acquired every 1 mm at 50kv, with 30 mA current and count time of 10 seconds.



ITRAX™ Micro X-ray Fluorescence Core Scanner settings for each 0.5 m long core.

| Sediment core | Bottom  | Top   | Voltage (kV) | Current (mA) | Step size (µm) | Section |
|---------------|---|---|--------------|--------------|----------------|---------|
| U969/ core 9  |  |  | 50           | 30           | 1000           | A/B     |
| U970/ core 8  |  |  | 50           | 30           | 1000           | B       |
| U971/ core 7  |  |  | 50           | 30           | 1000           | B/C     |
| U972/ core 6  |  |  | 50           | 30           | 1000           | C/D     |
| U973/ core 5  |  |  | 50           | 30           | 1000           | D       |
| U974/ core 4  |  |  | 50           | 30           | 1000           | D/E     |
| U975/ core 3  |  |  | 50           | 30           | 1000           | E       |
| U976/ core 2  |  |  | 50           | 30           | 1000           | E/F     |
| U977/ core 1  |  |  | 50           | 30           | 1000           | F/G     |

## Appendix 10: Micro- and macro fraction data

Micro- and macro- charcoal counts for 50 samples.

| Depth (cm) | Sample name | Macro (mm <sup>2</sup> cm <sup>-3</sup> ) | Micro (particles/cm <sup>3</sup> ) |
|------------|-------------|---|------------------------------------|
| 37         | ALEX 18-1   | 0.38225                                   | 17.25                              |
| 60         | ALEX 18-2   | 0.94875                                   | 10                                 |
| 94         | ALEX 18-3   | 1.6455                                    | 42.75                              |
| 120        | ALEX 18-4   | 1.83425                                   | 6.5                                |
| 157        | 5U3: po 12d | 3.63425                                   | 22.25                              |
| 164        | 5U3: po 11d | 11.13775                                  | 29.5                               |
| 168        | 5U3: po 10d | 6.03825                                   | 17.75                              |
| 172        | ALEX 18-5   | 1.224                                     | 20                                 |
| 177        | 5U3: po 9d  | 3.49475                                   | 7.75                               |
| 184        | 5U3: po 8d  | 2.21725                                   | 5.75                               |
| 197        | 5U3: po 7d  | 1.573                                     | 14.75                              |
| 202        | 5U3: po 6e  | 1.5915                                    | 7.75                               |
| 210        | 5U3: po 5e  | 6.8975                                    | 13                                 |
| 214        | ALEX 18-6   | 5.806                                     | 12.75                              |
| 217        | 5U3: po 4e  | 3.893                                     | 22                                 |
| 222        | 5U3: po 3e  | 3.43275                                   | 21.75                              |
| 231        | 5U3: po 2e  | 9.38                                      | 11                                 |
| 242        | 5U3: po 1e  | 5.748                                     | 7.75                               |
| 250        | 5U3: po 23e | 25.13775                                  | 14.5                               |
| 258        | 5U3: po 22e | 6.40575                                   | 14                                 |
| 264        | 5U3: po 21e | 7.3585                                    | 4                                  |
| 268        | 5U3: po 20e | 1.27025                                   | 2                                  |
| 274        | 5U3: po 19e | 3.006                                     | 9.5                                |
| 281        | 5U3: po 18e | 2.80525                                   | 7.5                                |
| 285        | ALEX 18-7   | 1.44825                                   | 8.5                                |
| 290        | 5U3: po 17e | 2.78675                                   | 0.5                                |
| 294        | 5U3: po 16e | 1.205                                     | 1.5                                |

## OSL and palaeoenvironmental proxies in Alexandra Cave, Naracoorte

|     |             |         |       |
|-----|-------------|---------|-------|
| 297 | 5U3: po 15e | 4.768   | 9.5   |
| 302 | 5U3: po 14e | 3.99225 | 14.5  |
| 308 | 5U3: po 13e | 5.42575 | 36    |
| 317 | 5U3: po 24e | 3.15775 | 6     |
| 325 | ALEX 18-8   | 0.05075 | 19.25 |
| 329 | 5U3: po 39f | 1.101   | 20.75 |
| 331 | 5U3: po 40f | 0.083   | 23.75 |
| 336 | 5U3: po 38f | 1.183   | 51.5  |
| 338 | 5U3: po 37f | 0.07075 | 28.5  |
| 341 | 5U3: po 36f | 2.77675 | 48    |
| 344 | 5U3: po 35f | 0.1115  | 22    |
| 347 | 5U3: po 34f | 0.01525 | 17    |
| 349 | 5U3: po 33f | 8.44    | 41    |
| 353 | 5U3: po 32f | 4.1815  | 56.75 |
| 357 | 5U3: po 31f | 9.0115  | 19.25 |
| 361 | 5U3: po 30f | 6.40875 | 31.5  |
| 365 | 5U3: po 29f | 0.369   | 17    |
| 368 | 5U3: po 28f | 1.61025 | 5.25  |
| 371 | 5U3: po 27f | 2.776   | 8     |
| 374 | ALEX 18-9   | 7.8655  | 31.5  |
| 377 | 5U3: po 26f | 1.52875 | 2     |
| 381 | 5U3: po 25f | 0.284   | 1.25  |
| 392 | ALEX 18-10  | 0.7985  | 2.5   |

**Appendix 11: Carbon isotope data**

Carbon isotope values and weight. Error is within  $\pm 1\sigma$  range.

| Sample name    | Depth | $\delta^{13}\text{C}$ | $\delta^{13}\text{C}$ err | mg C     | err      |
|----------------|-------|-----------------------|---------------------------|----------|----------|
| ALEX 18-1      | 37    | -25.6112              | 0.11                      | 42.08598 | 2.651417 |
| ALEX 18-1      | 37    | -18.4276              | 0.11                      | 58.40855 | 3.679738 |
| ALEX 18-1      | 37    | -23.3244              | 0.11                      | 21.82362 | 1.374888 |
| ALEX 18-1 bulk | 37    | -25.4402              | 0.11                      | 101.0606 | 6.366817 |
| ALEX 18-2      | 60    | -24.622               | 0.11                      | 15.70582 | 0.989466 |
| ALEX 18-2      | 60    | -24.9797              | 0.22                      | 10.19866 | 0.642516 |
| ALEX 18-2      | 60    | -24.4086              | 0.22                      | 9.368434 | 0.590211 |
| ALEX 18-2 bulk | 60    | -23.8482              | 0.11                      | 19.16294 | 1.207265 |
| ALEX 18-3      | 94    | -26.5116              | 0.11                      | 31.58139 | 1.989628 |
| ALEX 18-3      | 94    | -24.9757              | 0.11                      | 32.365   | 2.038995 |
| ALEX 18-3      | 94    | -26.3516              | 0.11                      | 32.94636 | 2.075621 |
| ALEX 18-3 bulk | 94    | -25.7332              | 0.11                      | 131.381  | 8.277002 |
| ALEX 18-4      | 120   | -23.7628              | 0.11                      | 70.7701  | 4.458516 |
| ALEX 18-4      | 120   | -25.0269              | 0.11                      | 29.71386 | 1.871973 |
| ALEX 18-4      | 120   | -25.7846              | 0.11                      | 178.123  | 11.22175 |
| ALEX 18-4 bulk | 120   | -25.3775              | 0.11                      | 189.0493 | 11.91011 |
| ALEX 18-5      | 172   | -24.77                | 0.11                      | 99.8944  | 6.293347 |
| ALEX 18-5      | 172   | -24.3859              | 0.11                      | 34.84884 | 2.195477 |
| ALEX 18-5      | 172   | -24.6913              | 0.11                      | 40.53559 | 2.553742 |
| ALEX 18-5 bulk | 172   | -24.8439              | 0.11                      | 118.8242 | 7.485927 |
| ALEX 18-6      | 202   | -24.8837              | 0.11                      | 179.0456 | 11.27987 |
| ALEX 18-6      | 202   | -25.8406              | 0.11                      | 114.2566 | 7.198164 |
| ALEX 18-6      | 202   | -24.9911              | 0.11                      | 66.34588 | 4.179791 |
| ALEX 18-6 bulk | 202   | -25.1763              | 0.11                      | 203.1598 | 12.79907 |
| ALEX 18-7      | 285   | -25.2735              | 0.11                      | 39.9426  | 2.516384 |
| ALEX 18-7      | 285   | -25.6038              | 0.11                      | 37.32118 | 2.351234 |
| ALEX 18-7      | 285   | -25.6871              | 0.11                      | 17.21154 | 1.084327 |

## OSL and palaeoenvironmental proxies in Alexandra Cave, Naracoorte

|                 |     |          |      |          |          |
|-----------------|-----|----------|------|----------|----------|
| ALEX 18-7 bulk  | 285 | -22.3062 | 0.11 | 49.68876 | 3.130392 |
| ALEX 18-8       | 325 | -23.9163 | 1.1  | 1.246278 | 0.078516 |
| ALEX 18-8       | 325 | -24.3184 | 0.44 | 2.737628 | 0.172471 |
| ALEX 18-8       | 325 | -22.8917 | 0.22 | 9.165257 | 0.577411 |
| ALEX 18-8 bulk  | 325 | -24.1718 | 0.11 | 80.86203 | 5.094308 |
| ALEX 18-9       | 374 | -27.8323 | 0.22 | 6.696307 | 0.421867 |
| ALEX 18-9       | 374 | -24.1605 | 0.11 | 47.54826 | 2.99554  |
| ALEX 18-9       | 374 | -25.5318 | 0.22 | 5.758567 | 0.36279  |
| ALEX 18-9 bulk  | 374 | -26.107  | 0.11 | 71.52862 | 4.506303 |
| ALEX 18-10      | 392 | -28.5799 | 0.22 | 8.441095 | 0.531789 |
| ALEX 18-10      | 392 | -25.2965 | 0.11 | 11.22977 | 0.707476 |
| ALEX 18-10      | 392 | -25.7252 | 0.22 | 9.30526  | 0.586231 |
| ALEX 18-10 bulk | 392 | -27.9089 | 0.11 | 71.70946 | 4.517696 |